The chemistrode: A droplet-based microfluidic device for stimulation and recording with high temporal, spatial, and chemical resolution

Delai Chen[a,1], Wenbin Du[a,1], Ying Liu[a,1], Weishan Liu[a,1], Andrey Kuznetsov[b], Felipe E. Mendez[b], Louis H. Philipson[b], and Rustem F. Ismagilov[a,2]

[a]Department of Chemistry and Institute for Biophysical Dynamics, University of Chicago, 929 East 57th Street, Chicago, IL 60637; and [b]Department of Medicine and the Kovler Diabetes Center, University of Chicago, 5841 South Maryland Avenue, Chicago, IL 60637

Edited by George M. Whitesides, Harvard University, Cambridge, MA, and approved September 15, 2008 (received for review August 19, 2008)

Microelectrodes enable localized electrical stimulation and recording, and they have revolutionized our understanding of the spatiotemporal dynamics of systems that generate or respond to electrical signals. However, such comprehensive understanding of systems that rely on molecular signals—e.g., chemical communication in multicellular neural, developmental, or immune systems—remains elusive because of the inability to deliver, capture, and interpret complex chemical information. To overcome this challenge, we developed the "chemistrode," a plug-based microfluidic device that enables stimulation, recording, and analysis of molecular signals with high spatial and temporal resolution. Stimulation with and recording of pulses as short as 50 ms was demonstrated. A pair of chemistrodes fabricated by multilayer soft lithography recorded independent signals from 2 locations separated by 15 μm. Like an electrode, the chemistrode does not need to be built into an experimental system—it is simply brought into contact with a chemical or biological substrate, and, instead of electrical signals, molecular signals are exchanged. Recorded molecular signals can be injected with additional reagents and analyzed off-line by multiple, independent techniques in parallel (e.g., fluorescence correlation spectroscopy, MALDI-MS, and fluorescence microscopy). When recombined, these analyses provide a time-resolved chemical record of a system's response to stimulation. Insulin secretion from a single murine islet of Langerhans was measured at a frequency of 0.67 Hz by using the chemistrode. This article characterizes and tests the physical principles that govern the operation of the chemistrode to enable its application to probing local dynamics of chemically responsive matter in chemistry and biology.

analysis | dispersion | flow | microscale | pulse

This article describes the "chemistrode," a droplet-based microfluidic device for manipulating and observing molecular signals with high spatial and temporal resolution. The microelectrode, voltage-clamp, and patch-clamp techniques (1) enabled stimulation and recording of electrical activity and redox-active molecules with high resolution in both space and time, revolutionizing our understanding of electroactive processes from biochemistry to neuroscience (1–3). Most biological processes, however, are fundamentally chemical rather than electrical, relying on molecular signals to orchestrate events at the correct time and location. Electrochemical approaches are widely used, but not all molecules are electrochemically active, and some electrochemically active molecules are difficult to measure selectively in complex mixtures. The grand challenge this article addresses is that of devising an analogue of the electrode that operates on molecular rather than electrical or electroactive signals.

Why could we not build such a system with today's technology? Whereas electrical signals travel through wires essentially instantly and with low losses, manipulation and transport of molecules is more challenging. First, a pulse of molecules, especially of small volume, rapidly disperses when transported through a tube by laminar flow, leading to loss of concentration and time resolution. Loss of molecules from solution by adsorption to surfaces of tubes may also occur. Therefore, methods that rely on laminar flow to transport molecular signals, such as direct sampling (4), push/pull perfusion (5), microdialysis (6), and direct microinjection, have not addressed this grand challenge. In contrast to electrical signals, molecular signals comprise multiple, often unknown, molecular species, requiring the ability to deliver multiple molecular species as stimuli and the ability to analyze a pulse of response molecules by multiple techniques. Advances in optical imaging technology, new probes and tagging methods, and photo-controllable manipulation have enabled observation and manipulation of many known molecular species, but these technologies may be time consuming to develop for each species and difficult to use for multiple or unknown species. "Biology on a chip" microfluidics technologies (7–9) can reduce dispersion by minimizing the distance that molecules are transported by the integration of a biological experiment with a specific analytical method. However, this approach requires the redevelopment and validation of the biological protocols as well as the miniaturization and integration of disparate analytical technologies. Recent advances in microfluidics have used multiphase flow to transport solutions reliably as discrete units without dilution, cross-contamination, or loss of temporal resolution (10–19).

We developed the chemistrode, a microfluidic platform that addresses this grand challenge by providing molecular stimulation and recording with high fidelity using plug-based (12) multiphase microfluidics [Fig. 1*A* and supporting information (SI) Fig. S1]. Like the electrode, the chemistrode is simply brought into contact with the surface under investigation, e.g., a cell or tissue. Instead of exchanging electrical signals, molecular signals are delivered by and captured in plugs, aqueous droplets nanoliters in volume surrounded by a fluorocarbon carrier fluid. The compartmentalization of these molecular signals eliminates dispersion and loss of sample due to surface adsorption (18).

Operation of the chemistrode relies on 9 general steps (Fig. 1 *A* and *B*): (*i*) preparation of an array of aqueous plugs containing an arbitrary sequence of stimuli (20, 21); (*ii*) delivery of the array of stimulus plugs to a hydrophilic substrate; (*iii*) coalescence of

Author contributions: D.C., W.D., Y.L., W.L., A.K., L.H.P., and R.F.I. designed research; D.C., W.D., Y.L., W.L., and F.E.M. performed research; D.C., W.D., Y.L., W.L., A.K., L.H.P., and R.F.I. analyzed data; and D.C., W.D., Y.L., W.L., and R.F.I. wrote the paper.

The authors declare no conflict of interest.

This article is a PNAS Direct Submission.

[1]D.C., W.D., Y.L., and W.L. contributed equally to this work.

[2]To whom correspondence should be addressed. E-mail: r-ismagilov@uchicago.edu.

This article contains supporting information online at www.pnas.org/cgi/content/full/0807916105/DCSupplemental.

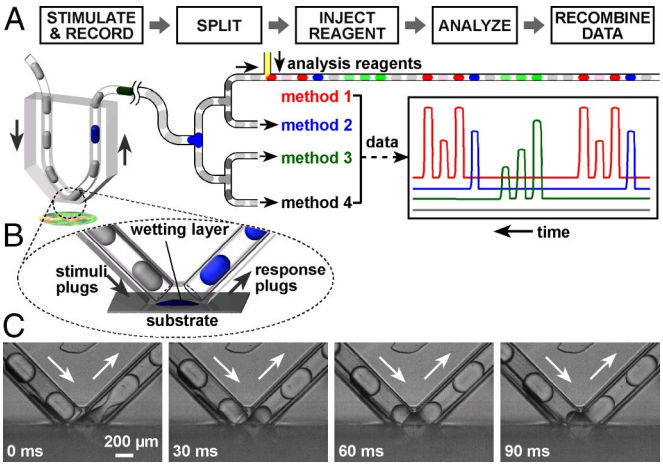

Fig. 1. The chemistrode delivers and records multiple molecular signals with high temporal and spatial resolution for off-line analysis by multiple analytical methods in parallel. (*A*) A conceptual schematic drawing of stimulation, recording, and analysis. See text for details. (*B*) Schematic of the chemistrode brought into contact with a hydrophilic substrate. (*C*) Time-lapse bright-field images (side view) of an incoming stimulus plug merging with the wetting layer above a hydrophilic glass surface and the formation of a response plug as the fluid exits the wetting layer (see Movie S1).

stimulus plugs with the wetting layer above the hydrophilic substrate (11) while the fluorocarbon carrier fluid remains in contact with the hydrophobic wall of the chemistrode; (*iv*) rapid exchange of diffusible signals between the plug and the wetting layer; (*v*) re-formation of plugs containing response molecules released by the substrate; (*vi*) delivery of response plugs to a splitting junction to form identical daughter arrays (22); (*vii*) injection of each daughter array with reagents required for further analysis (23); (*viii*) analysis of each daughter array by a different technique; and (*ix*) final recombination of data from the analysis of daughter arrays to provide a time-resolved record of molecular stimulation and response dynamics. Here, we describe the physical principles that guide the operation of the chemistrode and implement the chemistrode to test the feasibility of each step and the compatibility of this platform with living cells.

Results

To deliver pulses of stimuli and capture pulses of molecular signals as they are released with high temporal resolution and efficiency, the chemistrode must handle plugs at high frequency while ensuring coalescence of plugs with the wetting layer and efficient chemical exchange between a plug and the wetting layer. To characterize these parameters, we fabricated a chemistrode with a v-shaped channel (with 200- or 240-μm i.d. Teflon tubing inserted) by using rapid prototyping in poly(dimethylsiloxane) (PDMS) (Fig. 1*B* and Fig. S1) (24). Microchannels were rendered hydrophobic and fluorophilic by using silanization (25). By using high-speed video microscopy, steps *ii* through *v* were observed for the delivery and recording of buffer plugs on a hydrophilic glass surface (Fig. 1*C*). To achieve stable transport of plugs, the chemistrode must operate at a low value of the capillary number, $Ca = U\mu/\gamma < 0.1$, where U (m/s) is the flow velocity, μ (kg/m·s) is the dynamic viscosity, and γ (N/m) is the surface tension at the interface between the aqueous phase and the carrier fluid (26). Assuming the center-to-center distance between adjacent plugs to be 6 times d (m), the diameter of the channel (26), Ca limits the frequency f at which plugs can flow over a surface, f_{Ca} (s^{-1}), to $\frac{Ca\cdot\gamma}{\mu\cdot 6d}$, or $f_{Ca} \approx 0.17(\text{m/s})/d$. For the channels of the chemistrode used here, $d = 2 \times 10^{-4}$ m, corresponding to $f_{Ca} \approx 800\ s^{-1}$.

The pressure drop, ΔP (Pa), required to achieve these frequencies provides an additional constraint on frequency, $f_{\Delta P}$. By using the Hagen–Poiseuille equation as an approximation, for a channel with length L (m) long enough to hold N plugs, $L = 6Nd$, and $f_{\Delta P} = \frac{\Delta P}{6N \times 192\ \mu}$, independent of d. When $n = 100$ and $\Delta P \approx 10^5$ Pa, $f_{\Delta P} \approx 900\ s^{-1}$, but this value is the upper bound of $f_{\Delta P}$, because multiphase flow requires higher pressure drops than predicted by the Hagen–Poiseuille equation because of capillary pressure, Marangoni stresses, and a modification of the velocity profile inside the plugs (27).

To achieve rapid coalescence of the stimulus plug and the wetting layer (step *iii*), 3 factors must be considered (11, 28): (*i*) the rate of drainage of the carrier fluid to bring the wetting layer and the plug within a critical distance for coalescence, (*b*) the critical contact time between the wetting layer and the plug at the critical distance, and (*c*) surfactant dynamics (29, 30). Geometry of the chemistrode prevented the fusion of multiple droplets on the surface and chemical exchange among them. Although such fusion is a useful feature in some applications (11), it is undesirable for the chemistrode, because fusion introduces cross-contamination and reduces temporal resolution. We accelerated coalescence by using carrier fluids with low viscosity that can drain on the submillisecond time scale. We also used a small-molecule surfactant, triethyleneglycol mono[1H,1H-perfluorooctyl]ether (RfOEG) known to prevent nonspecific protein adsorption (25) to the aqueous–fluorous interface. This surfactant induced desirable surface tension and displayed sufficiently rapid dynamics to provide reliable frequencies of coalescence, $f_{coal} > 50\ s^{-1}$. By considering the parameters and conditions described above, the temporal resolution, t_{res} (s), can be estimated as $t_{res} \approx \frac{\phi}{f}$, where f is the limiting frequency (the lowest one among f_{Ca}, $f_{\Delta P}$, and f_{coal}), and ϕ is the unitless number of plugs necessary to exchange >95% of molecules of interest between plugs and the wetting layer (which was in the $\approx 10^1$- to 10^2-μm range in our experiments, depending on the geometry and flow rate).

To test the efficiency of chemical exchange between plugs and the wetting layer (step *iv*), high-speed fluorescence video microscopy was used to observe a fluorescent molecular signal delivered to a hydrophilic glass surface (Fig. 2*A*). We used small-molecule fluorescent dyes for simplicity and because many diffusible signals are small molecules. The fluorescent signal was encoded in 1 plug containing fluorescein, which was followed by many plugs of nonfluorescent buffer. This array was flowed into the chemistrode at a flow velocity of 4.2 mm/s, and an increase in fluorescence at the surface of the substrate was observed after the fluorescent plug coalesced with the wetting layer. The fluorescein in the wetting layer was rapidly removed by subsequent buffer plugs with $\phi = 3$ (Fig. 2*A*). Experimentally, the observed value of ϕ depended on the extent of recirculation induced as plugs coalesced with the wetting layer. The value of ϕ correlated with the value of $\sqrt{We}$, the square root of the dimensionless Weber number (24), which describes the ratio of fluid's inertia to surface tension driving recirculation (data not shown). $We = \rho U^2 d/\gamma$, where ρ (kg/m^3) is the density of the fluid. We quantified this effect by using the chemistrode to deliver an array of plugs of fluorescein to saturate the wetting layer, followed by an array of buffer plugs that removed fluorescein from the wetting layer (Fig. 2*B* and Fig. S2). As $\sqrt{We}$ increased from 0.0036 to 0.14, recirculation was reduced, and the value of ϕ decreased from 4 to 2. Viscosity of the plugs did not significantly affect the value of ϕ (data not shown), also suggesting that $\sqrt{We}$ is better than Ca or Re for describing ϕ. Mass transport by

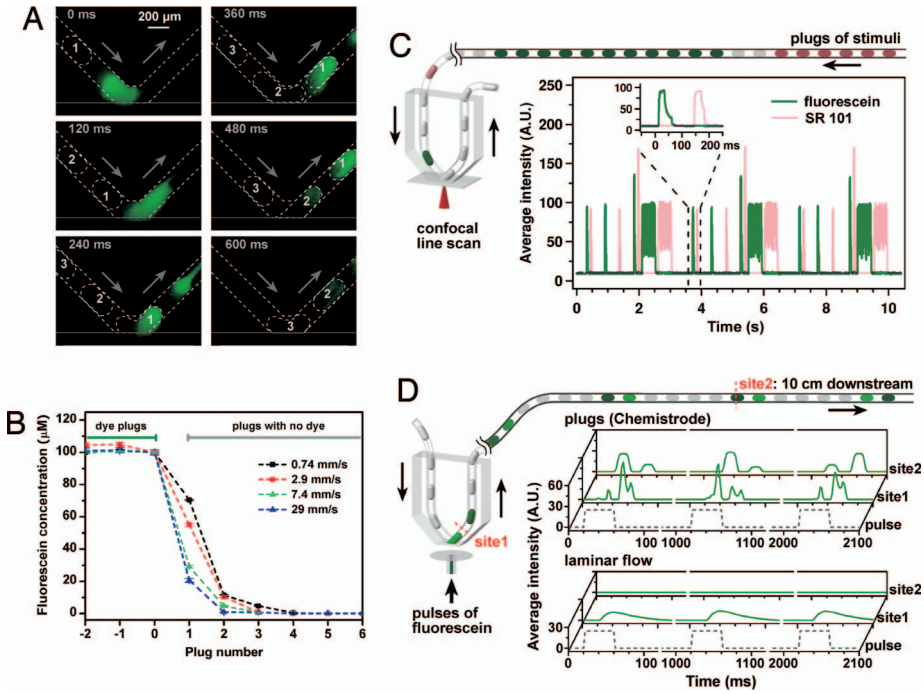

Fig. 2. The chemistrode provides stimulation and recording with high temporal resolution. (*A*) Time-lapse fluorescence images of the delivery and capture of fluorescein within the wetting layer by 3 buffer plugs. See Movie S2 for more details. (*B*) Removal of fluorescein from the wetting layer by buffer plugs as a function of flow velocity. Data indicate rapid mass transport between the wetting layer and the plugs. Error bars are standard deviation ($n = 5$) (see *SI Text*). (*C*) Stimulation with a preformed array of fluorescent plugs containing fluorescein (green), sulforhodamine 101 (red), and buffer (gray) detected at the wetting layer with a confocal microscope (schematic on the left, experimental data on the right). A.U., arbitrary units. (*D*) Intensity of recorded 40-ms pulses of fluorescein measured at the tip of the chemistrode (site 1) and 10 cm downstream (site 2) (schematic on the left). Experimental data (right, green graphs of fluorescence intensity) show that pulses (shown as dashed gray lines) are reliably captured at site 1 and transported 10 cm to site 2 by response plugs in the chemistrode (upper graph and Movie S3) but not by the single-phase laminar flow in the same device (lower graph and Movie S4).

diffusion near the surface did not limit the overall mass transport in those experiments, but it could become limiting for molecules with very low effective diffusion coefficients (e.g., because of large size or binding to cell surfaces or extracellular matrix). For systems where both mass transport and kinetics are slow, the flow may be stopped and restarted to allow plugs to collect more of the released molecules. Overall, these experiments predicted that a temporal resolution of ≈50 ms should be achievable in this geometry at higher flow velocities. Re-formation of response plugs (step *v*) took place reliably in the chemistrode at $Ca < 0.1$ and did not limit t_{res}.

Using the parameters described above, the chemistrode enabled delivery of an array of an arbitrary sequence of multiple molecular signals as pulses of controlled intensity and duration at high temporal resolution (Fig. 2*C* and Fig. S3). We delivered plugs of only 2 fluorescent dyes and imaged the wetting layer with 2 wavelengths simultaneously by using high-speed confocal microscopy. Short pulses with duration of ≈50 ms (width at half-height) were encoded in individual plugs, delivered at a frequency of 1 plug per 50 ms. Because long plugs may break up spontaneously, encoding of longer pulses was more reliable with sequences of short plugs. Higher-intensity pulses were encoded with plugs containing the reagent at higher concentration. The predetermined sequence of plugs was delivered 3 times with high reproducibility (Fig. 2*C*). This experiment confirmed efficient delivery of the reagents into the wetting layer, also observed in Fig. 2*A*. These results also demonstrated that the chemistrode is compatible with standard optical imaging techniques.

We hypothesized that the chemistrode would provide efficient recording of released signals superior to that of single-phase laminar flow. To simulate the release of molecules from a surface, fluorescein was pulsed out of a glass microcapillary tube that ended flush with the PDMS surface (Fig. 2*D*). The chemistrode was brought into contact with the wetting layer above the tip of the capillary tube. Pulses of ≈40 ms with a volume of 0.2 nL were generated every second and collected by using either the plug-based flow (at a frequency of 1 plug per ≈37 ms) of the chemistrode or single-phase laminar flow in the same geometry (Fig. 2*D* and Fig. S4). Fluorescence was detected at the tip of the device (site 1) and 10 cm downstream (site 2) by using high-speed fluorescence video microscopy. In these experiments, we were unable to measure fluorescence simultaneously at both sites. Therefore, the plots of fluorescence intensity shown for sites 1 and 2 are sequential but do not correspond to the same pulses. In the chemistrode at site 1, >95% of the fluorescent signal was distributed over no more than 2 plugs. Recirculation within plugs redistributed the contents of the pulse and caused the measured signal to fluctuate in some of the plugs (Movie S3). The recorded signal was transported 10 cm with no loss of temporal resolution. In contrast, recording with single-phase laminar flow resulted in poor temporal resolution and poor efficiency of collection. Broadening of the fluorescent peaks was already visible at the tip of the device (site 1, Movie S4), and the intensity of the signal decreased to <1% of the initial value after traveling 10 cm downstream (site 2) because of dispersion.

To test whether the chemistrode provided chemical stimulation and recording with spatial resolution of tens of micrometers—potentially important for work on the cellular and subcellular scales—we used multilayer soft lithography (31, 32) to fabricate a 2-layer chemistrode with 25-μm channels separated by a thin (15 μm) spacer of PDMS (Fig. 3*A* and Fig. S5). To simulate the release of molecules from a hydrophilic surface at 2 locations, we ejected pulses of any of 3 solutions through 2 (30 ± 2) × (20 ± 5)-μm orifices separated by 15 μm (Fig. 3*A*).

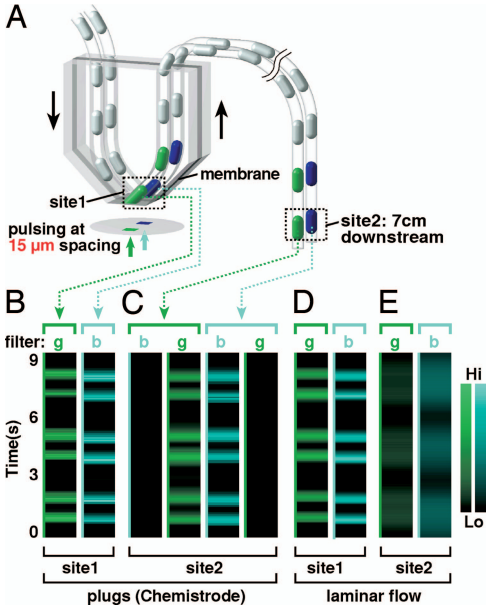

Fig. 3. An array of chemistrodes operates at high spatial resolution. (*A*) A schematic drawing of the 2-layer chemistrode device used for sampling 2 signals, 8-methoxypyrene-1,3,6 trisulfonic acid (MPTS, blue) or fluorescein (green), released through 2 orifices separated by 15 μm (see *SI Text*). (*B–E*) A plot of fluorescence intensity of the 2 fluorescent signals, observed through green (g) and blue (b) filters, captured and transported by plugs of the chemistrode (*B* and *C*) and laminar flow (*D* and *E*) in the same geometry.

The solutions were buffer (colorless), fluorescein (green), and 8-methoxypyrene-1,3,6 trisulfonic acid (MPTS, blue). We then brought the pair of chemistrodes in contact with the wetting layer above the orifices to record ejected pulses, and we detected fluorescence at the tip of the device (site 1) and 7 cm downstream (site 2). The 2-layer chemistrode reliably recorded the sequences of pulses at both locations (Fig. 3 *B* and *C*) with cross-contamination of $<1\%$ and no loss of intensity during transport (Fig. 3*C*). The use of plugs was essential—when single-phase laminar flow was used instead, pulses rapidly broadened, overlapped, and decayed (Fig. 3 *D* and *E*). In these small channels, Taylor dispersion was less severe, but losses to the walls of channels became pronounced, especially when we tested solutions of proteins. Because the carrier fluid completely encapsulates the aqueous plug and eliminates its contact with the walls, two-phase flow of the chemistrode reliably transported even molecules that tended to adsorb to PDMS and Teflon. We do not anticipate partitioning of hydrophobic or amphiphilic molecules from the aqueous plugs into the fluorocarbon carrier fluid, as shown in previous studies (33, 34).

To test the compatibility of the chemistrode with off-line, multianalyte measurements by independent methods (steps *vi–ix*), we used the chemistrode to record pulses of a mixture of 4 compounds—$CaCl_2$, insulin, glucose, and MPTS as a positive control—each representing a different class of molecules and detectable by a different technique (Fig. 4*A*). A mixture of these compounds was pulsed through the end of a Y-shaped channel. The chemistrode was brought into contact with the wetting layer above the channel. The array of recorded response plugs was split into 4 identical daughter arrays (step *vi*). Each plug in the first daughter array was injected (step *vii*) with a fluorescent indicator, fluo-4. Measuring fluorescence of the fluo-4-Ca^{2+} complex of each plug (step *viii*) in this array detected the presence of Ca^{2+} ions and provided a profile of Ca^{2+} release as a function of time (Fig. S6). In parallel, plugs in the second array were injected with the mixture of an anti-insulin antibody and labeled insulin for a competitive immunoassay with a 20 nM limit of detection, shown as the baseline in Fig. 4*B* and Fig. S7. Control experiments indicated that plugs provide an excellent transport and storage medium for insulin for off-line analysis with no losses of insulin due to degradation or adsorption to surfaces (25), in contrast to almost complete loss of insulin from laminar flow in the same Teflon tube. To determine the concentration of insulin, the fraction of labeled insulin that was free or bound to the antibody was detected by using fluorescence correlation spectroscopy (FCS) (35). Plugs in the third array were injected with Girard's reagent T [(carboxymethyl)trimethylammonium chloride hydrazide] and incubated overnight to give a hydrazone derivative of glucose, and the presence of the hydrazone was then detected by MALDI-MS (Fig. S8, a method that can detect unknown molecules. As a control, fluorescence of MPTS was measured in the fourth array. Analysis of insulin data indicated that $>98\%$ of the pulsed signal was recovered by the chemistrode. Final recombination of data from all 4 analyses (step *ix*) showed good alignment among different techniques and with the positive control trace of MPTS (Fig. 4*B*).

Splitting followed by off-line analysis (Fig. 4*A*) is an attractive feature of the chemistrode that decouples the stimulating and recording experiment from the equipment and expertise that may be required for analysis of nanoliter volumes. We demonstrated decoupling in time: Whereas the chemical signals were recorded on the time scale of seconds, incubation and measurement steps during analysis required >24 h but did not lead to loss of signal or time resolution. We also demonstrated decoupling in location: We performed recording with the chemistrode (Fig. 4*A*) in our laboratory and analyzed plugs for insulin 1 day later by using an FCS instrument located 20 miles away. Control experiments indicated that storage and transportation of tubing containing response plugs did not affect the time resolution or quality of analysis by FCS. Arrays of plugs have been shipped cross-country or frozen and thawed without disruption. The ability to deliver, record with no losses of resolution or concentration, duplicate, store, send by mail, and analyze by multiple techniques space- and time-resolved chemical information encoded as an array of plugs in a tube could dramatically enhance collaborations and use of unique analytical facilities.

Finally, we tested the compatibility of the chemistrode with live-cell experiments (Fig. 4*C*) by using mouse islets of Langerhans, a model system widely studied in the context of diabetes (36–38). Using the chemistrode, we stimulated single islets (Fig. 4*D*) by using a transition from a resting buffer containing 2 mM glucose to a stimulant buffer containing 14 mM glucose. The increase of intracellular $[Ca^{2+}]_i$ by islets in response to the stimulation was optically monitored (36) by measuring the fluorescence intensity of fluo-4. We observed regularly oscillating $[Ca^{2+}]_i$ in islets being stimulated with plugs of buffer containing 14 mM glucose for up to 1 h (Fig. S9). Next, by forming recording plugs at a frequency of 0.67 s^{-1} and measuring the insulin concentration in the recording plugs, we determined, every 1.5 s, the rate of insulin secretion of an islet under stimulation with solutions containing 30 mM KCl and 2 mM glucose. We chose these conditions to ensure rapid response dynamics and rapid secretion of insulin. We included a fluorescent dye, Alexa Fluor 594, as a marker in the stimulant plugs. To align the trace of off-line analysis to the $[Ca^{2+}]_i$ data, we used the transitions of marker intensity between the baseline and the plateau as the references and kept track of the position of every plug in the recording array. The intensity of Alexa Fluor 594 measured by fluorescent microscopy during stimulation agreed well with the intensity measured by off-line analysis of recorded plugs, indicating that temporal information was preserved by plugs. Upon stimulation, after a short $\approx$2-s delay, the islet displayed the expected response—a sharp increase of $[Ca^{2+}]_i$ accompanied by a burst of insulin release within $\approx$10 s (Fig. 4*E*).

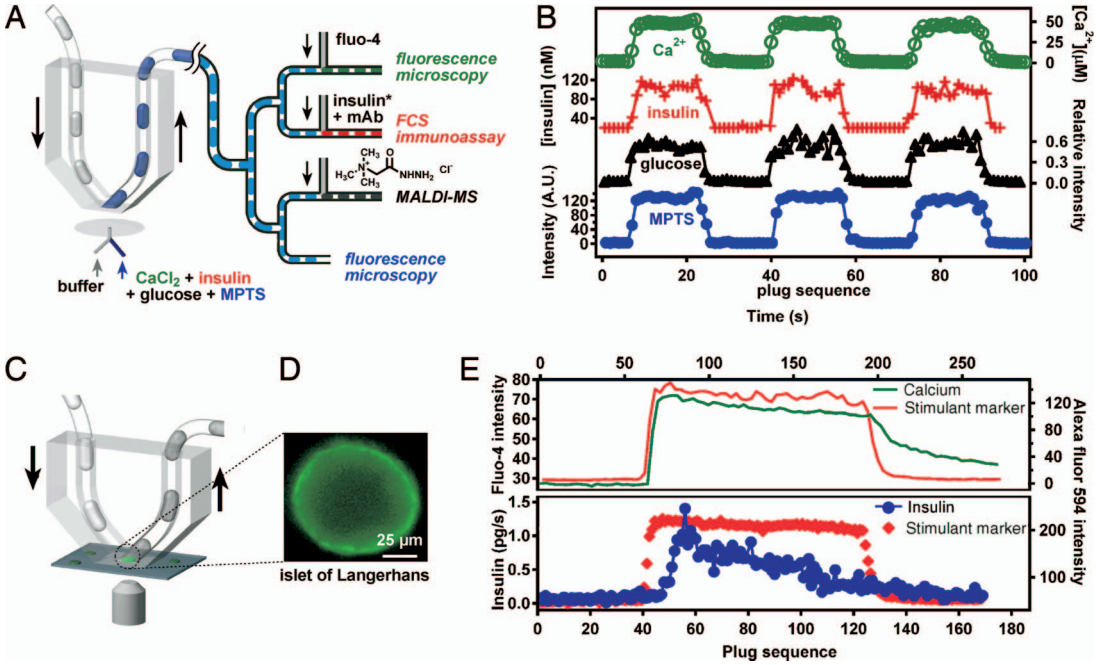

Fig. 4. The chemistrode is compatible with parallel off-line analysis by independent analytical techniques and is compatible with living cells as a substrate. (*A* and *B*): Use of the chemistrode to record and analyze pulses of sample solution containing $CaCl_2$, insulin, glucose, and a fluorescent dye, MPTS. (*A*) A schematic of the experiment. Pulses were generated at the surface. After recording with the chemistrode, recorded plugs were split into 4 identical daughter arrays for off-line analysis via fluorescence microscopy, FCS competitive immunoassay, and MALDI-MS. (*B*) Experimental data of Ca^{2+}, insulin, glucose, and MPTS analyses combined and aligned to reveal the complete release profile of the 4 species. (*C–E*) Use of the chemistrode to stimulate a mouse islet of Langerhans and record insulin secretion every 1.5 s. A.U., arbitrary units. (*C*) A schematic of the experiment. An islet was cultured on a glass-bottom dish, and the chemistrode was positioned over the islet. Stimulation and recording took place while the islet was imaged by fluorescence microscopy. (*D*) A fluorescent image of an islet showing an increase of fluorescence of fluo-4, corresponding to the rise in intracellular $[Ca^{2+}]_i$ in the islet upon stimulation. (*E*) Graphs showing the $[Ca^{2+}]_i$ response and insulin secretion of a stimulated mouse islet. (*Upper*) Traces measured by fluorescence microscopy during stimulation and recording, showing the fluorescence intensity of fluo-4 (green) as an indicator of $[Ca^{2+}]_i$ and the intensity of Alexa Fluor 594 (red) as a marker of the stimulant solution. (*Lower*) Traces with results of off-line analysis of plugs collected during recording, showing the fluorescence intensity of Alexa Fluor 594 marker and the calculated insulin secretion rate.

The peak rate of insulin secretion was in general agreement with those observed previously in islet-on-a-chip microfluidic experiments (38), and the rapid dynamics of secretion are consistent with stimulation by a solution of high KCl concentration. The response was also reproduced for different batches of healthy islets and agreed with that observed in control experiments, confirming that the chemistrode did not introduce artifacts. The compatibility of the chemistrode with live-cell experiments is consistent with compatibility of single-phase, aqueous microfluidic devices widely used in experiments with living cells (7, 8, 36), with the design of chemistrode that brings only the aqueous phase in contact with the cell, whereas the fluorocarbon remains in contact with the walls of the device, and with compatibility of fluorocarbons with living cells and tissues (39).

Discussion

One may speculate that, ultimately, the ability to contact the surface of a sample at a specific location and deliver molecular stimuli and then record, store, and analyze the pulses of molecules released in response could enable truly fascinating experiments in chemistry and biology. Molecular signals could be recorded "in stereo" from multiple locations on a surface with high spatial resolution, capturing a conversation among cells or revealing differences in secretion at different regions of the same cell. A sequence of pulses of molecular signals recorded with high temporal resolution from one cell could be played back to another cell with high fidelity or manipulated to identify the sequence of molecular signals essential to induce a particular function. These and other stimulation-recording-analysis experiments could advance areas that rely on extracellular communication, from dynamics of biofilms, to development of multicellular organisms, to signaling in neural circuits, to hormonal regulation.

The chemistrode has not yet been used to carry out such speculative experiments, because, as this article describes, there are physical principles and limitations governing the operation of the chemistrode. Obviously, many opportunities remain to further advance the chemistrode. For example, what operating ranges of the chemistrode are compatible with particular living cells and tissues? Can nanoporous membranes be integrated to control the shear experienced by the substrate while providing rapid mass transfer between the substrate and the plugs? For signaling molecules that show slow mass transfer because of binding to extracellular matrices, what are the best approaches to prevent or reverse this binding, or locally disrupt the matrices? How can pressure-sensitive valves be incorporated to balance pressure at the substrate? How can mechanically stable microprobes be fabricated for insertion into tissues? What are the best analytical techniques for each application, and what is the optimal way of integrating them? How can this approach be integrated with advances in laminar-flow-based probes (9, 40–42)? The spatial resolution of the chemistrode is not yet at the level demonstrated by carbon fiber- and nanotube-based approaches (43); how can the chemistrode be scaled down further to operate in the patch-clamp mode on a single channel or to capture single secretory vesicles? As these questions are answered, the chemistrode should advance chemistry of responsive materials (44, 45), surface catalysis (46), and understanding of biological systems that are intrinsically responsive to stimuli and display nontrivial spatial and temporal dynamics on levels ranging from networks (47) to cells (48) to tissues (49, 50).

Materials and Methods

See *SI Text* for materials, more detailed procedures, and additional data.

Fabrication and Operation of Microfluidic Devices. All microfluidic devices were fabricated by rapid-prototyping soft lithography in PDMS (24). Surfaces of microchannels were made hydrophobic and fluorophilic by silanization (*SI Text*) (25). The chemistrode device was fabricated by inserting connecting Teflon microcapillaries into the 2 arms of a V-shaped channel. Arrays of stimulant plugs were generated by using a microfluidic device according to previously reported procedures (20) or a home-built robotic system (*SI Text*). Gastight syringes (series 1700; Hamilton) with removable 27-gauge needles and 30-gauge Teflon tubing (Weico Wire and Cable) were used to load aqueous solutions and carrier fluid. PHD 2000 infusion syringe pumps (Harvard Apparatus) controlled with LabVIEW (National Instruments) programs were used to drive flows.

Supporting Information. The following procedures are described in *SI Text*: characterization of the temporal and spatial resolution of stimulation and recording by using the chemistrode with fluorescent dyes; analysis of insulin, Ca^{2+}, glucose, and MPTS; and the monitoring of insulin secretion from single mouse islets.

ACKNOWLEDGMENTS. We thank Vytas Bindokas for help with confocal microscopy and Jessica M. Price for contributions in writing and editing this manuscript. This work was supported by National Institutes of Health (NIH) Director's Pioneer Award 1DP1OD003584 and National Science Foundation (NSF) Collaborative Research in Chemistry Grant CHE-0526693 (to R.F.I.), NIH Grants DK48494, DK63493, and DK20595 (to L.H.P.) and the Blum–Kovler Foundation (L.H.P.). R.F.I. is a Cottrell Scholar of Research Corporation and a Camille Dreyfus Teacher–Scholar. A part of this work was performed at the Materials Research Science and Engineering Center microfluidic facility funded by the NSF.

1. Hamill OP, Marty A, Neher E, Sakmann B, Sigworth FJ (1981) Improved patch-clamp techniques for high-resolution current recording from cells and cell-free membrane patches. *Pflugers Arch* 391:85–100.
2. Hubel DH, Wiesel TN (1959) Receptive fields of single neurones in the cats striate cortex. *J Physiol (London)* 148:574–591.
3. Wightman RM (2006) Probing cellular chemistry in biological systems with microelectrodes. *Science* 311:1570–1574.
4. Kennedy RT, Thompson JE, Vickroy TW (2002) In vivo monitoring of amino acids by direct sampling of brain extracellular fluid at ultralow flow rates and capillary electrophoresis. *J Neurosci Methods* 114:39–49.
5. Cellar NA, Burns ST, Meiners JC, Chen H, Kennedy RT (2005) Microfluidic chip for low-flow push–pull perfusion sampling in vivo with on-line analysis of amino acids. *Anal Chem* 77:7067–7073.
6. Stuart JN, Hummon AB, Sweedler JV (2004)The chemistry of thought: Neurotransmitters in the brain. *Anal Chem* 76:120A–128A.
7. El-Ali J, Sorger PK, Jensen KF (2006) Cells on chips. *Nature* 442:403–411.
8. Atencia J, Beebe DJ (2005) Controlled microfluidic interfaces. *Nature* 437:648–655.
9. Sabounchi P, *et al.* (2006) Soft-state biomicrofluidic pulse generator for single cell analysis. *Appl Phys Lett* 88:183901.
10. Anna SL, Bontoux N, Stone HA (2003) Formation of dispersions using ''flow focusing'' in microchannels. *Appl Phys Lett* 82:364–366.
11. Fidalgo LM, Abell C, Huck WTS (2007) Surface-induced droplet fusion in microfluidic devices. *Lab Chip* 7:984–986.
12. Song H, Tice JD, Ismagilov RF (2003) A microfluidic system for controlling reaction networks in time. *Angew Chem Int Ed* 42:768–772.
13. Lorenz RM, Edgar JS, Jeffries GDM, Chiu DT (2006) Microfluidic and optical systems for the on-demand generation and manipulation of single femtoliter-volume aqueous droplets. *Anal Chem* 78:6433–6439.
14. Garstecki P, Fuerstman MJ, Stone HA, Whitesides GM (2006) Formation of droplets and bubbles in a microfluidic T-junction—Scaling and mechanism of break-up. *Lab Chip* 6:437–446.
15. Link DR, *et al.* (2006) Electric control of droplets in microfluidic devices. *Angew Chem Int Ed* 45:2556–2560.
16. Wang M, Roman GT, Schultz K, Jennings C, Kennedy RT (2008) Improved temporal resolution for in vivo microdialysis by using segmented flow. *Anal Chem* 80:5607–5615.
17. Sahoo HR, Kralj JG, Jensen KF (2007) Multistep continuous-flow microchemical synthesis involving multiple reactions and separations. *Angew Chem Int Ed* 46:5704–5708.
18. Song H, Chen DL, Ismagilov RF (2006) Reactions in droplets in microflulidic channels. *Angew Chem Int Ed* 45:7336–7356.
19. Huebner A, *et al.* (2008) Microdroplets: A sea of applications? *Lab Chip* 8:1244–1254.
20. Zheng B, Ismagilov RF (2005) A microfluidic approach for screening submicroliter volumes against multiple reagents by using preformed arrays of nanoliter plugs in a three-phase liquid/liquid/gas flow. *Angew Chem Int Ed* 44:2520–2523.
21. Zheng B, Ismagilov RF (2005) A microfluidic approach for screening submicroliter volumes against multiple reagents by using preformed arrays of nanoliter plugs in a three-phase liquid/liquid/gas flow. *Angew Chem* 117:2576–2579.
22. Adamson DN, Mustafi D, Zhang JXJ, Zheng B, Ismagilov RF (2006) Production of arrays of chemically distinct nanolitre plugs via repeated splitting in microfluidic devices. *Lab Chip* 6:1178–1186.
23. Li L, Boedicker JQ, Ismagilov RF (2007) Using a multijunction microfluidic device to inject substrate into an array of preformed plugs without cross-contamination: Comparing theory and experiments. *Anal Chem* 79:2756–2761.
24. Duffy DC, McDonald JC, Schueller OJA, Whitesides GM (1998) Rapid prototyping of microfluidic systems in poly(dimethylsiloxane). *Anal Chem* 70:4974–4984.
25. Roach LS, Song H, Ismagilov RF (2005) Controlling nonspecific protein adsorption in a plug-based microfluidic system by controlling interfacial chemistry using fluorous-phase surfactants. *Anal Chem* 77:785–796.
26. Tice JD, Song H, Lyon AD, Ismagilov RF (2003) Formation of droplets and mixing in multiphase microfluidics at low values of the Reynolds and the capillary numbers. *Langmuir* 19:9127–9133.
27. Adzima BJ, Velankar SS (2006) Pressure drops for droplet flows in microfluidic channels. *J Micromech Microeng* 16:1504–1510.
28. Bibette J, Calderon FL, Poulin P (1999) Emulsions: Basic principles. *Rep Prog Phys* 62:969–1033.
29. Rekvig L, Frenkel D (2007) Molecular simulations of droplet coalescence in oil/water/surfactant systems. *J Chem Phys* 127.
30. Pawar Y, Stebe KJ (1996) Marangoni effects on drop deformation in an extensional flow: The role of surfactant physical chemistry. 1. Insoluble surfactants. *Phys Fluids* 8:1738–1751.
31. Anderson JR, *et al.* (2000) Fabrication of topologically complex three-dimensional microfluidic systems in PDMS by rapid prototyping. *Anal Chem* 72:3158–3164.
32. Unger MA, Chou HP, Thorsen T, Scherer A, Quake SR (2000) Monolithic microfabricated valves and pumps by multilayer soft lithography. *Science* 288:113–116.
33. Li L, *et al.* (2006) Nanoliter microfluidic hybrid method for simultaneous screening and optimization validated with crystallization of membrane proteins. *Proc Natl Acad Sci USA* 103:19243–19248.
34. Hatakeyama T, Chen DLL, Ismagilov RF (2006) Microgram-scale testing of reaction conditions in solution using nanoliter plugs in microfluidics with detection by MALDI-MS. *J Am Chem Soc* 128:2518–2519.
35. Haustein E, Schwille P (2007) Fluorescence correlation spectroscopy: Novel variations of an established technique. *Annu Rev Biophys Biomolec Struct* 36:151–169.
36. Rocheleau JV, Walker GM, Head WS, McGuinness OP, Piston DW (2004) Microfluidic glucose stimulation reveals limited coordination of intracellular Ca2+ activity oscillations in pancreatic islets. *Proc Natl Acad Sci USA* 101:12899–12903.
37. Ma L, *et al.* (2004) Direct imaging shows that insulin granule exocytosis occurs by complete vesicle fusion. *Proc Natl Acad Sci USA* 101:9266–9271.
38. Dishinger JF, Kennedy RT (2007) Serial immunoassays in parallel on a microfluidic chip for monitoring hormone secretion from living cells. *Anal Chem* 79:947–954.
39. Matsumoto S, Kuroda Y (2002) Perfluorocarbon for organ preservation before transplantation. *Transplantation* 74:1804–1809.
40. Juncker D, Schmid H, Delamarche E (2005) Multipurpose microfluidic probe. *Nat Mater* 4:622–628.
41. Olofsson J, *et al.* (2005) A chemical waveform synthesizer. *Proc Natl Acad Sci USA* 102:8097–8102.
42. Takayama S, *et al.* (2001) Laminar flows—Subcellular positioning of small molecules. *Nature* 411:1016.
43. Chen X, Kis A, Zettl A, Bertozzi CR (2007) A cell nanoinjector based on carbon nanotubes. *Proc Natl Acad Sci USA* 104:8218–8222.
44. Beebe DJ, *et al.* (2000) Functional hydrogel structures for autonomous flow control inside microfluidic channels. *Nature* 404:588–590.
45. Kost J, Langer R (2001) Responsive polymeric delivery systems. *Adv Drug Deliv Rev* 46:125–148.
46. Roeffaers MBJ, *et al.* (2006) Spatially resolved observation of crystal-face-dependent catalysis by single turnover counting. *Nature* 439:572–575.
47. Kastrup CJ, Runyon MK, Shen F, Ismagilov RF (2006) Modular chemical mechanism predicts spatiotemporal dynamics of initiation in the complex network of hemostasis. *Proc Natl Acad Sci USA* 103:15747–15752.
48. Huse M, Lillemeier BF, Kuhns MS, Chen DS, Davis MM (2006) T cells use two directionally distinct pathways for cytokine secretion. *Nat Immunol* 7:247–255.
49. Shea SD, Margoliash D (2003) Basal forebrain cholineraic modulation of auditory activity in the zebra finch song system. *Neuron* 40:1213–1226.
50. Ismagilov RF, Maharbiz MM (2007) Can we build synthetic, multicellular systems by controlling developmental signaling in space and time? *Curr Opin Chem Biol* 11:604–611.

Supporting Information

Chen *et al.* 10.1073/pnas.0807916105

SI Text

Materials. Unless otherwise stated, all chemicals were purchased at standard grades and used as received. FC3283 (3M) was used as the carrier fluid with surfactant 1,1,2,2-tetrahydroperfluorooctanol (PFO; Alfa Aesar) or RfOEG (triethyleneglycol mono[1*H*,1*H*-perfluorooctyl]ether), which was prepared according to published procedures (1). Human insulin and albumin from bovine serum (BSA) were purchased from Sigma–Aldrich. Monoclonal antibody to human insulin was purchased from Meridian Life Science. Tween 20 and 2,5-dihydroxybenzoic acid were purchased from Acros Organics. Alexa Fluor 488 5-TFP, cell-impermeant fluo-4 pentapotassium salt, cell-permeant fluo-4 a.m. ester, dextran Alexa Fluor 594, and 8-methoxypyrene-1,3,6 trisulfonic acid (MPTS) were purchased from Invitrogen. Chelex 100 resin was purchased from Bio-Rad. PTFE tubing was purchased from Zeus Industrial Products.

Fabrication and Use of the Chemistrode. To make the chemistrode, we first fabricated an enclosed V-shaped channel (300 × 300 μm) by rapid prototyping in poly(dimethylsiloxane) (PDMS) with geometry shown in Fig. S1*A*. Microchannels were rendered hydrophobic and fluorophilic by flowing tridecafluoro-1,1,2,2-tetrahydrooctyl-1-trichlorosilane vapor into the device for 1 h (1). Second, the device was carefully cut by a blade along the red dashed lines shown in Fig. S1*A*. Subsequently, Teflon tubing was inserted into the channels as shown in Fig. S1*B*. The gap between the Teflon tubing and surrounding PDMS was filled with half-cured PDMS glue (Dow–Corning Sylgard 184 A and B at a ratio of 10:1, cured at 110 °C for 110 s), and then the device was baked at 65 °C for the PDMS glue to fully cure. The tip of the chemistrode could be cut smaller, typically with a bottom area of ≈1 × 0.6 mm, to reduce the outer dimension.

To use the chemistrode, the inlet tubing was connected to a plug-generating device or a premade cartridge (see *Device and Methods for Fig. 1 and Fig. 2*, below). The chemistrode was held by a clamp of an x-y-z micromanipulator, and brought into contact with the surface supporting the substrate. A slight pressure toward the interface was applied to prevent leakage.

Solution Properties and Calculations of Weber Number and f_{Ca}. Properties of all aqueous solutions, including PBS buffer (1×, pH 7.4) and potassium phosphate buffer (32 mM, pH 8.2), were estimated as the values of water at room temperature. Viscosity and density of all aqueous solutions were estimated as 10^{-3} kg/(m·s) and 10^3 kg/m^3, respectively. Viscosity and density of FC3283 at room temperature were 1.4×10^{-3} kg/(m·s) and 1.82×10^3 kg/m^3, respectively. Surface tension of potassium phosphate buffer and FC3283 containing 0.5 mg/mL RfOEG was ≈10 mN/m. Weber number, *We*, is calculated as $We = \frac{\rho U^2 d}{\gamma}$, where ρ (kg·m^{-3}) is the density of the aqueous solution, d (m) is the tubing diameter, and γ (N·m^{-1}) is surface tension between the aqueous solution and the carrier fluid. U (m·s^{-1}) is the average flow velocity, which is calculated by $U = \frac{4Q}{\pi d^2}$, where Q (m^3·s^{-1}) is the volumetric flow rate. The capillary number, *Ca*, limits the frequency at which plugs can flow over a surface, f_{Ca}. f_{Ca} can be calculated by using the following experimental parameters.

$$f_{Ca} = \frac{Ca \cdot \gamma}{\mu \cdot 6d} = \frac{0.1 \times 10 \times 10^{-3}\text{N/m}}{10^{-3}\text{kg/(m·s)} \times 6 \times 200 \times 10^{-6}\text{m}} \approx 800\text{s}^{-1}.$$

Device and Methods for Fig. 1 and Fig. 2. ***Device and methods for Fig. 1C.*** Stimulus plugs were generated in a 3-inlet PDMS device with microchannels of square cross-section (100 μm) (Fig. S1*C*). The carrier fluid was 0.5 mg/mL RfOEG dissolved in FC3283. Plugs were formed by using an aqueous stream of buffer (32 mM potassium phosphate, pH 8.2) and an aqueous stream of 140 μM fluorescein dissolved in the same buffer. To generate repeated arrays of a single fluorescent plug followed by ≈20 nonfluorescent plugs, the carrier fluid stream was flowed continuously at a flow rate of 4 μL/min while a LabVIEW program switched between 2 aqueous streams in an alternating fashion. At any time, only 1 aqueous stream was flowing at a flow rate of 4 μL/min. The total flow rate was 8 μL/min. The resulting plugs were delivered to the chemistrode through PTFE tubing (200 μm i.d., 250 μm o.d.). Images were taken by using a high-speed Phantom 7.1 camera (Vision Research) at 1,000 fps (Movie S1). Four images from Movie S1 are shown in Fig. 1*C*.

Fig. 2A and Movie S2. Plugs were generated by using the same device, solutions, and program as above. Time-lapse fluorescent images were taken by using an inverted fluorescence microscope (IRE2; Leica) equipped with the high-speed Phantom camera at 500 fps (Movie S2).

Fig. 2B. Arrays of stimulus plugs were generated robotically (Fig. S3*A*) in 40-cm-long Teflon tubing (240 μm i.d.) and delivered to a hydrophilic glass surface through a chemistrode at various flow velocities. The volume of individual aqueous plugs and the carrier fluid between 2 plugs were both 30 nL. Calibration plugs containing different concentrations of fluorescein (sequence as recorded in Fig. S2*B*) were included at the beginning of each array, so that the fluorescence intensity could be quantitatively converted back into fluorescein concentration. The sequence of the calibration array was 10 plugs of 0 μM fluorescein in PBS buffer, 10 plugs of 25 μM fluorescein in PBS buffer, 10 plugs of 50 μM fluorescein in PBS buffer, and 10 plugs of 100 μM fluorescein in PBS buffer. After the calibration array, 5 cycles of stimulus plugs were repeated, where each cycle consisted of 5 fluorescent plugs (100 μM fluorescein in PBS buffer), followed by 20 nonfluorescent plugs (PBS buffer). The change in fluorescence intensity in the center of the wetting layer during the transition from fluorescent to nonfluorescent plugs was used to characterize the recording efficiency (Fig. S2*A*).

The fluorescence intensity on the surface of the substrate was monitored by using an inverted fluorescence microscope (IRE2; Leica), and images were acquired by using the Phantom camera. The images (Fig. S2*A*) were analyzed by using MetaMorph 6.0. Data were taken as the average intensity of a 200-μm-diameter circle at the center of the substrate as shown in Fig. S2*A*, because we assumed that the region of interest corresponded to stimuli located in the center of the area under the tip of the chemistrode. Each calibration data point was the average of 10 plugs. Each data point in Fig. 2*B* represents the average concentration of fluorescein in plugs from 5 cycles of stimulus plugs. The data obtained with the chemistrode at flow rate of 7.4 mm/s is shown in Fig. S2*B*, including average intensities of the time-lapse images and a calibration curve for converting intensity into concentration of fluorescein.

Fig. 2C. To deliver a sequence of multiple molecular signals, an array of plugs as shown in Fig. S3*B* was generated in PTFE tubing (240 μm i.d.) robotically as shown in Fig. S3*A*. Light-green, dark-green, light-red, and dark-red plugs contained 10 μM fluorescein, 20 μM fluorescein, 10 μM sulforhodamine 101, and 20 μM sulforhodamine 101, respectively. Gray plugs contained

only buffer. The volume of individual aqueous plugs and the carrier fluid between 2 plugs were both 30 nL. The carrier fluid was FC3283 containing 0.5 mg/mL RfOEG. Buffer for all aqueous solutions was potassium phosphate buffer (32 mM, pH 8.2). One array of plugs contained multiple repeating periods of the sequence. The chemistrode was brought into contact with a hydrophilic glass slide. Plugs in the preformed array were flowed into the chemistrode at a flow rate of 80 μL/min (flow velocity = 29 mm/s).

A Leica SP5 tandem scanner spectral 2-photon confocal microscope was used to obtain fluorescence data with the following settings: xt scan mode; pinhole (Airy) 1.3; zoom 4.9; HCX PL APO CS 10.0 × 0.40 DRY UV objective; laser lines of 488-nm Ar and 561-nm diode; emission bandwidths of 500.0–545.0 nm and 600.2–720.1 nm; 8-bit PMT output. A Leica LAS AF Lite (1.7.0 build 1240) was used to control the microscope and analyze the data. Focus was adjusted on the surface of the glass slide, determined by reflected light. The position of the line scan is shown in Fig. S3*C*. The scan rate was 8,000 lines per second. Every 8 lines were averaged for 1 recording time point. Two beams of laser (488 and 561 nm) were switched by an acoustic optical tunable filter (AOTF). Emission light of 500.0–545.0 nm and 600.2–720.1 nm were detected by 2 photomultiplier tube (PMT) fluorescence detectors. Fluorescence intensities of both fluorescein and sulforhodamine 101 were averaged on the center 50% along the lengths of line scans (Fig. S3*D*), which corresponded to a physical length of ≈150 μm.

Fig. 2D. To simulate the release of molecular signals from a surface, fluorescein solution was pulsed out of a microcapillary to a glass surface. A 5-cm-long fused silica capillary with square cross-section (50 μm i.d.; Polymicro Technologies) was placed in a PDMS channel. The gap between the capillary and surrounding PDMS was filled with PDMS glue as described above. The other end of the capillary was connected to a 20-cm-long Teflon tubing (300 μm i.d.) filled with fluorescein (500 μM), and this tubing was connected to a microinjector (IM300; Narishige). The chemistrode was brought into contact with the wetting layer above the opening of the capillary.

Stimulus plugs were formed by injecting both a carrier fluid stream (0.5 mg/mL RfOEG in FC3283) and an aqueous stream (1× PBS buffer, pH 7.4) into a T-junction (Fig. S4*A*). The volumetric flow rate of both streams was 16 μL/min, and the total flow rate was 32 μL/min. The microinjector delivered multiple pulses of fluorescein solution into the silica surface with well-defined injection time and intervals. A LabVIEW program was used to control the microinjector for automatic operation. The duration for each injection was 40 ± 2 ms, as measured by the recorded movie (Movie S3). The time interval between consecutive pulses was 1 s. Pulses of fluorescein collected by response plugs in the chemistrode were detected at 2 positions: the tip of the chemistrode (site 1) and 10 cm downstream (site 2) (Fig. S4*A*). In a separate experiment, pulses of fluorescein were also collected by single-phase laminar flow at a flow rate of 32 μL/min in the same device geometry. The detection results from the chemistrode were compared with those from the single-phase laminar flow at the same sites. The fluorescence microscopic images (Fig. S4 *B* and *C*) and movie (Movie S3 and Movie S4) were acquired by using a Leica IRE2 fluorescence microscope with the Phantom camera.

Device and Methods for Fig. 3. The PDMS microfluidic device for achieving high spatial resolution (Fig. S5*A*) was fabricated by using rapid-prototyping multilayer soft lithography (2). Two molds with mirrored channel designs (Fig. S5 *B* and *C*) were made. The tips of the chemistrode and the end of pulsing device were connected in these molds. The channels had uniform thickness of 25 μm and widths of 15 or 25 μm. Dow–Corning Sylgard 184 A and B components were mixed at a mass ratio of 5:1, poured onto the mold for the top layer to a thickness of 5 mm, and incubated at 65 °C for 30 min. A 20:1 mixture of A and B was spin-coated onto the mold for the second layer pattern at 3,600 rpm for 30 s and then cured at 65 °C for 25 min. This spin-coating resulted in a thin PDMS layer of ≈35 μm thick covering the channel patterns (membrane layer). This membrane layer was aligned to the top layer with a MJB3 contact Mask Aligner (Karl Suss) and cured at 65 °C for 15 min. The bonded layers were peeled from the mold, punched with access holes, sealed to a 1-mm-thick 5:1 (A/B) flat PDMS layer (preincubated the same as the top layer), and baked at 65 °C overnight. Finally, the chemistrode and the pulsing device were cut apart under a microscope by using a sharp blade. The spatial resolution was defined as the distance between the 2 closest corners of the 2 pulsing channels (Fig. S5*F*, ≈15 μm). By controlling the thickness of the membrane layer and the alignment of the 2 chemistrodes, we can get different spatial resolution ranging from ≈10 μm to hundreds of micrometers.

Before use, the pulsing device was made hydrophilic by injecting 5 mg/mL BSA solution in 1× PBS buffer (pH 7.4) into the pulsing channels at a flow rate of 0.1 μL/min for 30 min. Then, the pulsing channels were rinsed with PBS buffer to flush away residual BSA. This also made the surface (Fig. S5*F*) of the pulsing device, which was brought into contact with the chemistrode, hydrophilic. The channels of the chemistrode were rendered fluorophilic by flowing FC3283/PFO (5:1 vol/vol) into the chemistrode at a flow rate of 0.10 μL/min for 20 min to saturate the PDMS surface with fluorinated carrier fluid-phase surfactant.

For spatial resolution experiments, a clamp was used to bring the chemistrode and the pulsing device into close proximity (Fig. S5 *D* and *E*). Syringes filled with solution and carrier fluid were connected to the pulsing channels with Teflon tubing (300 μm i.d.) and driven by 4 syringe pumps (PHD2000; Harvard Apparatus) controlled by a LabVIEW program. Each pump simultaneously drove 2 syringes that were connected to the 2 different layers, ensuring simultaneous flow control in both layers of chemistrodes and pulsing devices (Fig. S5 *E* and *G*). An adjustable vacuum (adjusted to 50 ± 25 mmHg) was connected to the outlet channels of the chemistrode to balance the pressure drop at the tip of the chemistrode. Stimulus plugs were formed by flowing a carrier fluid stream (20% vol/vol PFO in FC3283) and an aqueous stream (1× PBS buffer, pH 7.4) into the T-junction at flow rates of 0.075 μL/min and 0.075 μL/min, respectively (Fig. S5*B*). For fluorescence measurements, a Leica DMIRE2 microscope with a digital camera (ORCA-ER; Hamamatsu) was used. GFP and DAPI filter cubes were used to observe the fluorescence of fluorescein and MPTS, respectively.

Device and Methods for Fig. 4. ***Preparation of solutions.*** Hepes buffer (25 mM) was made by diluting 0.1 M Hepes buffer (pH 7.35) with Millipore filtered water. This Hepes buffer was stirred with Chelex 100 resin for 1 h to reduce the background Ca^{2+} ions. A solution of 0.1% Tween 20 in 25 mM Hepes buffer was treated by Chelex 100 resin with the same protocol. The sample solution contained 250 μM $CaCl_2$, 500 nM insulin, 10 μM MPTS, 50 mM glucose, and 0.1% Tween 20 in 25 mM Hepes buffer. All solutions were filtered with 0.45-μm medium PTFE syringe filters (Fisher Scientific) before use. The concentration of insulin stock solution was quantified by using light absorption at 277 nm. All PDMS devices were rinsed with 50 μM EDTA and then Millipore filtered water before experiments.

Fig. 4A recording of pulses of multiple molecules. Stimulus plugs were formed by flowing a carrier fluid stream (0.5 mg/mL RfOEG in FC3283) and an aqueous stream (25 mM Hepes buffer, pH 7.35) into a T-junction at flow rates of 2.5 μL/min and 2.0 μL/min, respectively. The resulting plugs were transported through the chemsitrode device at a flow rate of 4.5 μL/min. Pulses of

chemicals were delivered to a hydrophilic surface through a 15 × 25-μm orifice from a single layer PDMS device shown in Fig. S5*C*. Alternating pulses of buffer (0.1% Tween 20 in 25 mM Hepes buffer, pH 7.35) or sample solution (250 μM $CaCl_2$, 500 nM human insulin, 10 μM MPTS, 50 mM glucose, and 0.1% Tween 20 in 25 mM Hepes, pH 7.35) were delivered to the surface at a flow rate of 0.5 μL/min and duration of 8 s. The chemistrode was aligned and brought into contact with the outlet of the pulsing device, and the pulses were captured in response plugs. Under these experimental conditions, the volume of response plugs had a 1:1 ratio to the volume of carrier fluid in the resulting array. After recording, the response plugs were split (3) into 4 identical daughter arrays in Teflon tubing (100 μm i.d.) for further analysis as discussed below. On the basis of flow rates and the starting concentrations of the sample, the concentrations in the response plugs (assuming 100% sample recovery) should be: 50 μM $CaCl_2$, 100 nM human insulin, and 2.0 μM MPTS. The average determined concentrations in response plugs were: 44 μM $CaCl_2$, 102 nM human insulin, and 2.0 μM MPTS.

Fig. 4B detection of Ca^{2+}. The analyzing agent for detecting Ca^{2+} contained 400 μM cell-impermeable fluo-4 pentapotassium salt, 400 nM dextran Alexa Fluor 594, and 0.1% Tween 20 in 25 mM Hepes buffer (pH 7.35). This solution of reagent was injected into each plug of 1 daughter array with the average injection ratio of 0.5. The injection ratio is the ratio between the volume of injected reagent and the volume of the plug before injection. The device used for injection was the same as described in previous publications (4). Briefly, the device consisted of a PDMS T-junction with a hydrophilic glass capillary inserted in the vertical arm of the "T." Reagent solutions were injected into plugs through the hydrophilic glass capillary. The intensities of fluo-4-Ca^{2+} complex, dextran Alexa Fluor 594, and MPTS in each plug were measured by using a Leica DMI6000 fluorescence microscope with GFP, Texas red, and DAPI filter cubes, respectively. MetaMorph 6.0 was used to control the microscope and analyze the data.

To obtain a calibration curve for the concentration of Ca^{2+} in the response plugs, cartridges of calibration plugs containing solutions made as shown in Fig. S6*A* were generated. Each of the calibration plugs was injected with analyzing reagent used in the analysis of response plugs. Then, the intensities of fluo-4-Ca^{2+} complex and dextran Alexa Fluor 594 were measured.

The concentration of Ca^{2+} in the response plugs was calibrated and corrected by following the procedure below:

(*i*) Calculating the fraction of the analyzing reagent injected:

$$\text{InjectionFraction} = \frac{I_{\text{Alexa594,postinjection}}}{I_{\text{Alex594,preinjection}}},$$

where $I_{\text{Alexa594,preinjection}}$ is the intensity of Alexa 594 in the analyzing reagent before injection, and $I_{\text{Alexa594, postinjection}}$ is the intensity of Alexa 594 in the plugs after injection.

(*ii*) Correcting the intensity of fluo-4-Ca^{2+} by subtracting the background intensity of the analyzing reagent:

$$I_{Ca^{2+},\text{corrected}} = I_{\text{original},Ca^{2+}} - I_{\text{background,analyzingagent}} \times \text{InjectionFraction}.$$

where $I_{Ca2+,\text{corrected}}$ is the corrected intensity of fluo-4-Ca^{2+}, $I_{original,Ca2+}$ is the original intensity of fluo-4-Ca^{2+} measured in the plugs after injection, and $I_{\text{background,analyzingagent}}$ is the intensity of fluo-4-Ca^{2+} in the analyzing reagent before injection.

(*iii*) Calculating the final concentration of Ca^{2+} in the calibration plugs after injection:

$$c_{Ca^{2+},\text{calibration,postinjection}} = c_{Ca^{2+},\text{calibration}} \times (1 - \text{InjectionFraction}),$$

where $c_{\text{Ca2+,calibration,postinjection}}$ is the final concentration of Ca^{2+} in calibration plugs after injection, and $c_{\text{Ca2+,calibration}}$ is the concentration of Ca^{2+} in calibration plugs before injection, equal to those in Fig. S6*A*.

(*iv*) By plotting $c_{\text{Ca2+,calibration,postinjection}}$ versus the corresponding fluorescence intensity of fluo-4-Ca^{2+}, a calibration curve of Ca^{2+} was obtained (Fig. S6*B*).

(*v*) By using the calibration curve and the intensity of fluo-4-Ca^{2+} in the response plugs, the concentration of Ca^{2+} in each response plug after injection ($c_{\text{Ca2+,sample,postinjection}}$ was obtained.

(*vi*) Finally, concentration of Ca^{2+} in the response plugs before injection ($c_{\text{Ca2+,sample}}$) was obtained.

$$c_{Ca^{2+},\text{sample}} = \frac{c_{Ca^{2+},\text{sample,postinjection}}}{1 - \text{InjectionFraction}}.$$

The ntensity of MPTS in each could be corrected as well:

$$I_{\text{MPTS,corrected}} = \frac{I_{\text{original,MPTS}}}{1 - \text{InjectionFraction}},$$

where $I_{\text{MPTS, corrected}}$ is the corrected intensity of MPTS, and $I_{\text{original, MPTS}}$ is the original measured intensity of MPTS.

Fig. 4B competitive immunoassay for insulin analysis. Labeled human insulin (insulin*) was prepared by reacting human insulin and Alexa Fluor 488 5-TFP according to the manufacturer's instructions. The resulting product was purified by HPLC to obtain a single pure monolabeled isomer (insulin*). The lypholized powder of insulin* was dissolved in 1× PBS buffer (pH 7.4) to a concentration of 40 μM and stored at −78 °C as 1-μL aliquots. To perform the immunoassay, a reagent solution containing 72 nM monoclonal anti-insulin antibody (mAb), 1.2 nM insulin*, 0.3% BSA, and 0.3% Tween 20 in 25 mM Hepes (pH 7.35) was injected into each plug of 1 daughter array. The procedure for injecting reagents into plugs was the same as that described above for Ca^{2+} detection. The flow rate was 0.60 μL/min for the array of response plugs and 0.15 μL/min for the reagent solution. The volumetric ratio of plugs to injected reagent was ≈2:1. The insulin and insulin* compete for binding to the mAb, thus changing the fraction of free insulin* in the solution. Insulin concentration was inferred by determining the fraction of free insulin* by using fluorescence correlation spectroscopy (FCS).

The plugs containing reagents and sample were analyzed by FCS performed by using a commercial instrument, ConfoCor 3 (Carl Zeiss). A 488-nm argon laser was used as the excitation light. BP 505–540 IR* was used as the emission filter. For FCS measurements on a plug, the curved carrier fluid–aqueous interface and the thin layer of carrier fluid surrounding the plugs could introduce artifacts. To avoid these potential problems, a coverglass-PDMS device was constructed to house the plug during FCS measurements (Fig. S7*A*). The device was fabricated by sealing a piece of PDMS with imprinted channels on the bottom surface to a no. 1 cover glass on both its top and bottom surfaces. The bottom cover glass formed an enclosed channel with the PDMS. The 2 ends of the PDMS channel were connected to Teflon tubing (100 μm i.d., 150 μm o.d.) to transport plugs in and out of the device. The center of the channel formed a chamber with dimensions of 50 μm (height) × 150 μm (width) × 350 μm (length) (Fig. S7*A*). This geometry of the chamber was chosen so that plugs become "flat," with minimal curvature of the aqueous–carrier fluid interface and minimal thickness of carrier fluid at the center of the bottom surface of the plug. Sealing both the top and bottom of the PDMS piece to the cover glass was also important to prevent the cover glasses from bending after sealing to the PDMS. FCS measurements were performed by focusing the light at the center of the plug and 25 μm above the cover glass–liquid interface.

Control experiments indicated that performing FCS in this geometry did not introduce artifacts due to the aqueous–carrier fluid interface.

Next, the characteristic diffusion time for free insulin* and insulin*-mAb were determined under these experimental conditions. First, FCS measurements were obtained for a solution of insulin* in the absence of mAb. A single-component 3D free-diffusion model was used to fit the autocorrelation curve and obtain the characteristic diffusion time of free insulin*. Next, FCS measurements were obtained for a series of solutions containing insulin* and increasing concentrations of mAb. The autocorrelation curves were fit by using a 2-component 3D free-diffusion model with the diffusion time of free insulin* fixed to give the characteristic diffusion time of the insulin*–mAb complex. In these experiments, the characteristic diffusion time was 60 μs and 230 μs for free insulin* and insulin*–mAb, respectively.

To analyze an array of response plugs, the plugs were carefully moved into the PDMS-cover glass chamber by using a manual syringe pump. After 1 plug arrived in the chamber, the flow was stopped, and FCS measurements were performed on the plug in the chamber. After the measurement, the plug was moved out of the chamber, and the next plug was moved into the chamber for measurement. The autocorrelation curves were fit with a 2-component (free insulin* and insulin*–mAb complex), 3D free-diffusion model to give 2 parameters: the average number of fluorescent insulin* molecules in focal volume and the fraction of insulin* unbound to mAb (free insulin*%). To determine the concentration of insulin, 4 calibration curves of free insulin*% at different concentrations of insulin were constructed, with the average number of insulin* molecules in the focal volume being 0.65, 0.75, 0.95, and 1.2, respectively (Fig. S7*B*).

Fig. 4B detection of glucose. The analyzing reagent for detecting glucose contained 0.1 M Girard's reagent T, 2% acetic acid, and 20 mM arabinose. This analyzing reagent was injected into each plug of 1 daughter array of response plugs with a volumetric ratio of plugs to injected reagent of 2:1. The procedure for injecting reagents into plugs was the same as that described above for Ca^{2+} detection. Glucose reacted with the Girard's reagent T to form a hydrazone (as illustrated below), resulting in increased detection sensitivity in MALDI-MS (5).

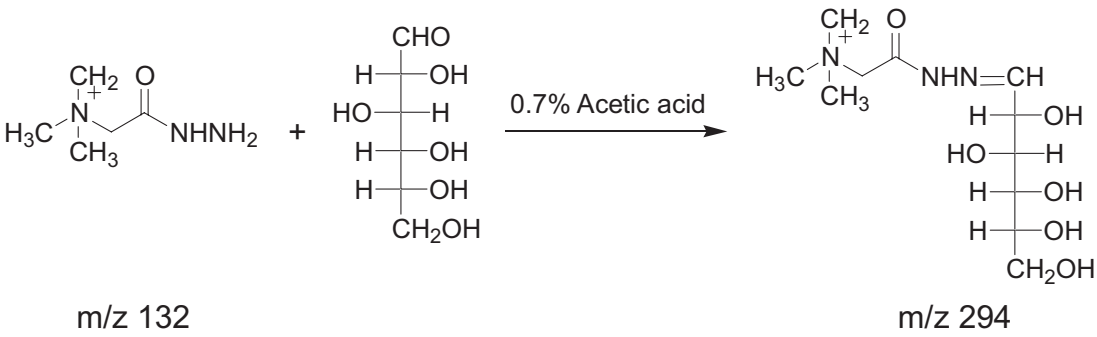

After incubation at room temperature for 60 h, each response plug was deposited onto a MALDI plate (plate type: ABI 01–192-6-AB, 192-well; Applied Biosystems) and allowed to evaporate. A matrix solution containing 10 mg/mL 2,5-dihydroxybenzoic acid in 1:1 acetonitrile/ethanol was deposited over each sample, which was dried and analyzed by MALDI-MS. MALDI spectra were acquired by using an ABI 4700 MALDI TOF/TOF MS instrument (Applied Biosystems).

All spectra were obtained with the same instrument settings: MS Reflector Positive operation mode; automatic acquisition control; acquisition mass range 100–350 Da; focus mass 213 Da; total shots per spectrum 3,000; fixed laser intensity 4,000 V; default calibration type. The peak heights in MALD-MS were measured with Data Explorer version 4.8 (Applied Biosystems). The level of glucose in each response plug was presented as the ratio of the peak height of hydrazone of glucose (*m*/*z* 294) to the peak height of Girard's reagent T (*m*/*z* 132). Representative MALDI-MS spectra are shown in Fig. S8.

Fig. 4 C–E experiments monitoring insulin secretion of single islets by the chemistrode. Islets were isolated from the pancreas of C57BL/6J wild-type mice (The Jackson Laboratory), 8–12 weeks of age, by using collagenase digestion and Ficoll gradients by following procedures described in previously published literature (6). Isolated islets were transferred to glass-bottom culture dishes (Mattek Corporation) and cultured in RPMI medium 1640 supplemented with 10% FBS, 2 mM L-glutamine, 100 units/mL penicillin, and 100 μg/mL streptomycin. Islets were maintained in a humidified incubator at 37 °C under an atmosphere of 95% air and 5% CO_2 and were used within 3 days of isolation.

Experiments to test compatibility of chemistrode with mouse islets are described below. Islets were loaded with fluo-4 (a calcium indicator) by incubating in Krebs–Ringer buffer (KRB) (119 mM NaCl, 4.7 mM KCl, 2.5 mM $CaCl_2$, 1.2 mM $MgSO_4$, 1.5 mM KH_2PO_4, 25 mM Hepes, pH 7.35) containing 5 μM cell permeable fluo-4 a.m., and 2 mM glucose for 40 min. The MatTek plate containing loaded islets was placed on a DMI6000 Leica fluorescence microscope that was kept at 37 °C. The staining medium was then replaced with KRB containing 2 mM glucose. A chemistrode was pressed down on the cover glass of MatTek plate by using a micromanipulator to trap 1 islet under the tip of the chemistrode. The PDMS tip of the chemistrode formed a conformal contact with the cover glass to isolate the space in the tip of the chemistrode from the bulk solution. Droplets of KRB containing either 2 mM glucose or 30 mM KCl plus 2 mM glucose plus 400 nM dextran Alexa Fluor 594 were formed and transported through the chemistrode by using the setup shown in Fig. 4*C*. All aqueous solutions and carrier fluid were oxygenated. The flow rates of the carrier fluid (0.5 mg/mL RfOEG in FC3283) and the aqueous stream were both 0.5 μL/min, resulting in a plug being delivered to the islet every 2 s. Time-lapse images of the islet under stimulation were captured with a DMI6000 Leica microscope every 3 s by using GFP and Texas red filter cubes. The incident excitation light was attenuated with an optical density 2.0 neutral density filter to reduce photo damage to the islet. Images were analyzed by using MetaMorph 6.0. Whereas data in the GFP channel recorded the $[Ca^{2+}]_i$ response of the islet under stimulation, intensity in the Texas red channel marked the aqueous solution being applied to the islet. Only the high glucose solution contained 400 nM dextran Alexa Fluor 594.

Concentration of insulin in the recording plugs were analyzed

as described above, with the following exceptions. The monoclonal antibody to insulin (CBL71) was purchased from Millipore. The standard sample of mouse insulin was extracted from mouse islets by soaking purified mouse islets in 1% Triton surfactant, followed by repeated freezing and thawing, and centrifugation to remove the debris. The concentration of insulin in the extracted sample was determined using an ELISA kit (ALPCO). Calibration curves were constructed by using appropriate concentrations of Alexa Fluor 488-labeled human insulin, antibody, and standard mouse insulin sample. When analyzing the concentration of insulin in the recording plugs, fluorescence of Alexa Fluor 594 was also detected. Only recording plugs of stimulant solution contained Alexa Fluor 594. Temporal profiles of $[Ca^{2+}]_i$ and insulin secretion were aligned by using Alexa Fluor 594 as the marker.

We confirmed the compatibility of the chemistrode with living cells for experiment with longer time scale. A continuous stimulation by plugs of KRB containing 14 mM glucose plus 400 nM dextran Alexa Fluor 594 was applied to the islets for 1 h through the chemistrode. The $[Ca^{2+}]_i$ response of the islet was imaged as described above. The islets displayed the expected $[Ca^{2+}]_I$ response—a slight decrease in $[Ca^{2+}]_i$, followed by a sharp increase and then a gradual decrease, followed by regular oscillations (Fig. S9).

1. Roach LS, Song H, Ismagilov RF (2005) Controlling nonspecific protein adsorption in a plug-based microfluidic system by controlling interfacial chemistry using fluorous-phase surfactants. *Anal Chem* 77:785–796.
2. Unger MA, Chou HP, Thorsen T, Scherer A, Quake SR (2000) Monolithic microfabricated valves and pumps by multilayer soft lithography. *Science* 288:113–116.
3. Adamson DN, Mustafi D, Zhang JXJ, Zheng B, Ismagilov RF (2006) Production of arrays of chemically distinct nanolitre plugs via repeated splitting in microfluidic devices. *Lab Chip* 6:1178–1186.
4. Chen DLL, Li L, Reyes S, Adamson DN, Ismagilov RF (2007) Using three-phase flow of immiscible liquids to prevent coalescence of droplets in microfluidic channels: Criteria to identify the third liquid and validation with protein crystallization. *Langmuir* 23:2255–2260.
5. Gouw JW, Burgers PC, Trikoupis MA, Terlouw JK (2002) Derivatization of small oligosaccharides prior to analysis by matrix-assisted laser desorption/ionization using glycidyltrimethylammonium chloride and Girard's reagent T. *Rapid Commun Mass Spectrom* 16:905–912.
6. Philipson LH, *et al.* (1994) Delayed rectifier K+ channel overexpression in transgenic islets and beta-cells associated with impaired glucose responsiveness. *J Biol Chem* 269:27787–27790.

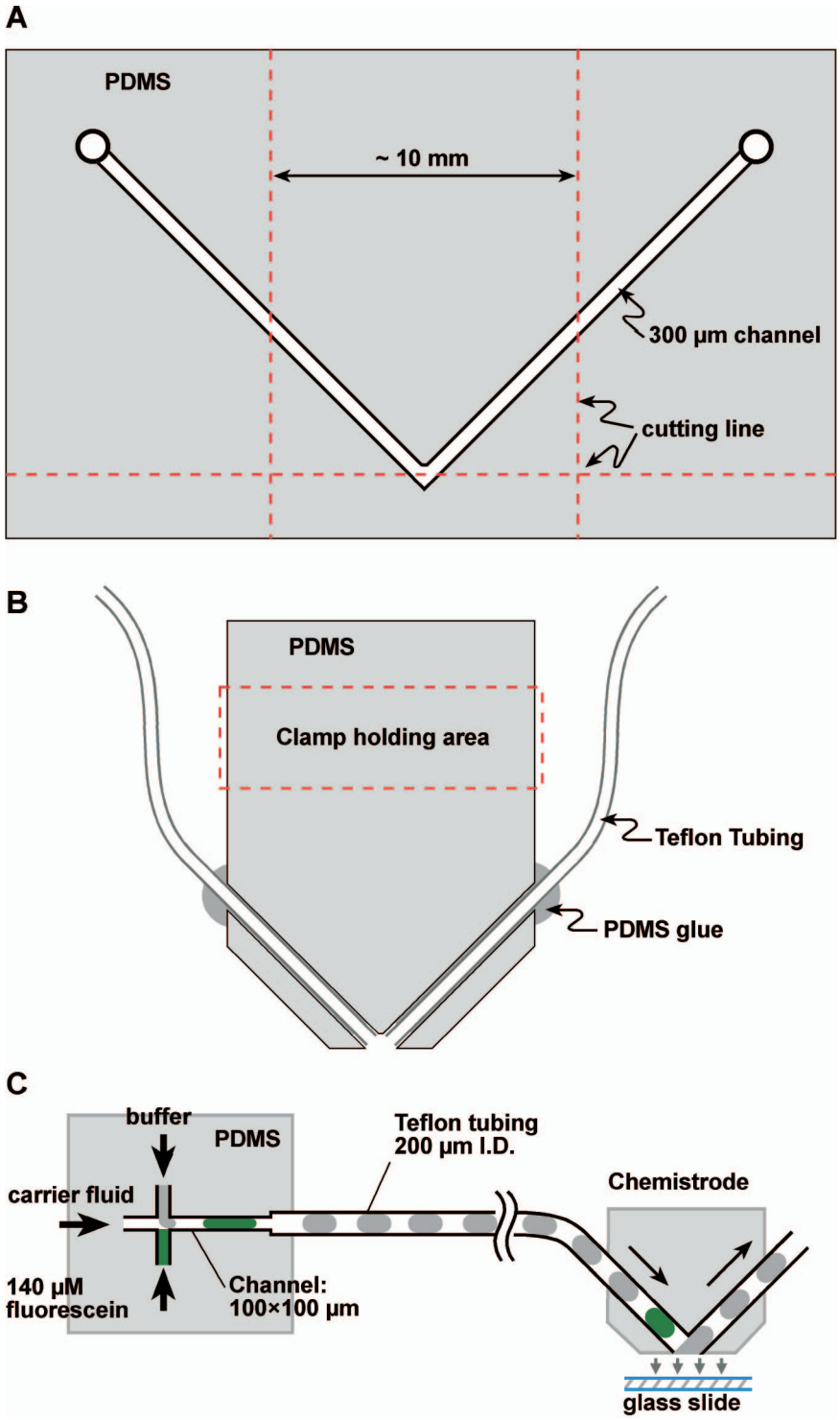

Fig. S1. Frabication and assembly of the chemistrode. (*A*) Design of the PDMS device of chemistrode. (*B*) An assembled chemistrode. (*C*) Schematic of the experimental setup for Figs. 1*C* and 2*A*.

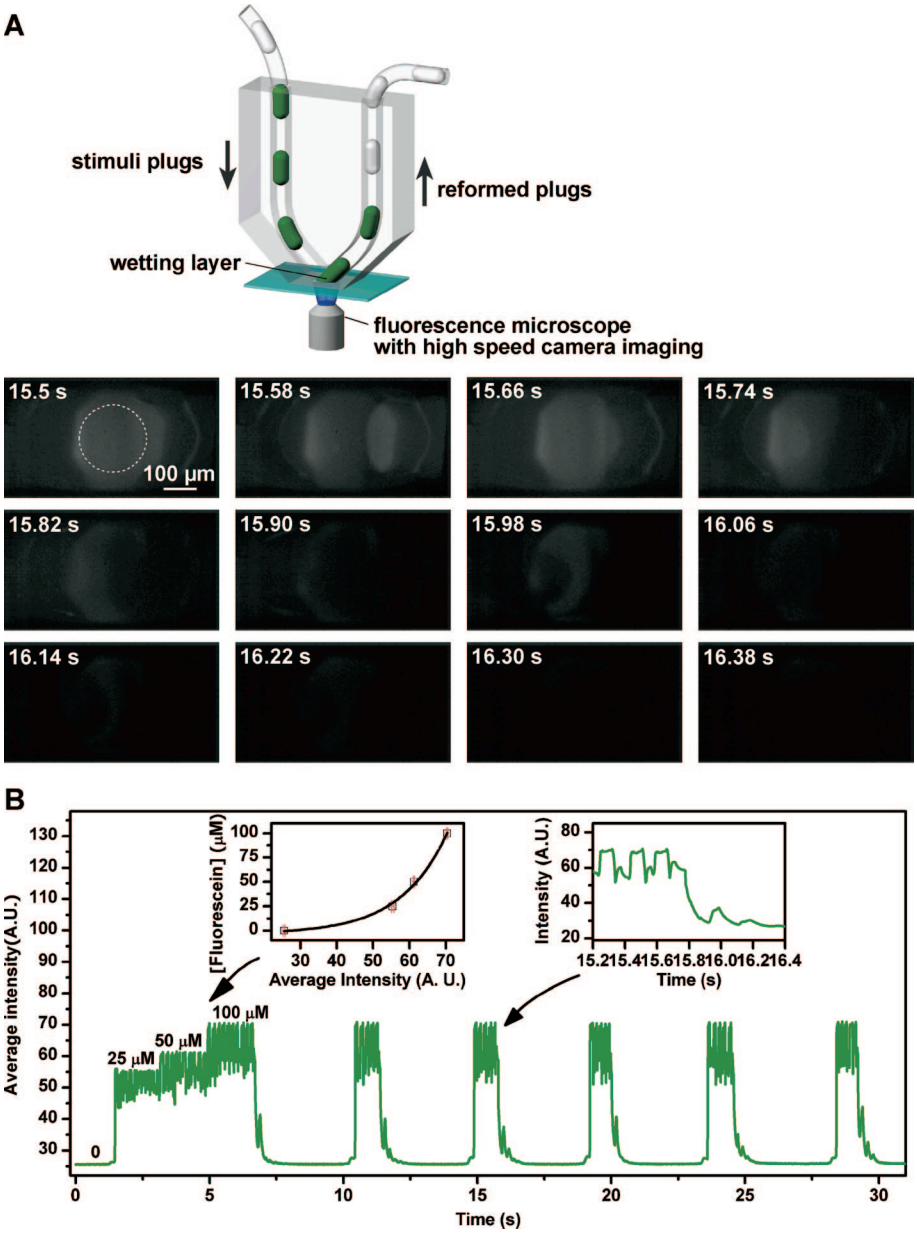

Fig. S2. Experimental setup and supporting data for Fig. 2*B*. (*A*) Schematic drawing of the experimental setup (*Upper*). Time-lapse fluorescence images of the removal of fluorescein from the wetting layer by subsequent buffer plugs at flow velocity of 7.4 mm/s are shown (*Lower*). These images were taken from below the substrate and were focused on the center of the wetting layer. The dashed circle in the first microscopic image indicates the region from which the data in Fig. 2*B* were extracted. (*B*) Fluorescence intensity measured from below the substrate as a preformed array of plugs containing fluorescein or buffer flowed over the substrate. Flow velocity: 7.4 mm/s. See *Device and Methods for Fig. 1 and Fig. 2* for more details. The *Inset* on the left shows the calibration curve for determining fluorescein concentration in the wetting layer. The *Inset* on the right shows a zoomed-in view of the fluorescence-intensity decrease during the transition from fluorescent to nonfluorescent plugs.

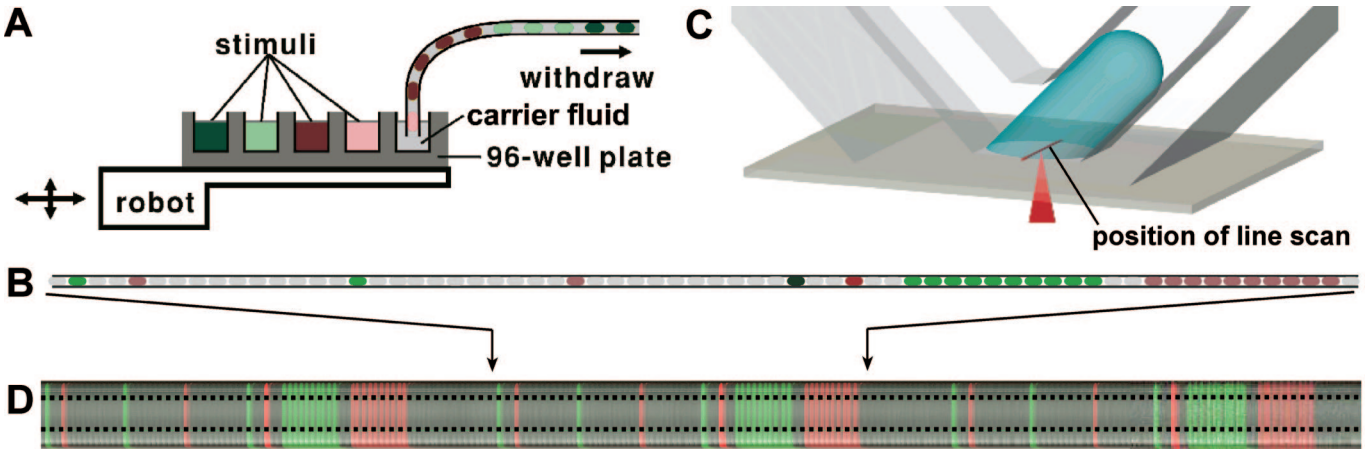

Fig. S3. Experimental design for Fig. 2*C*. (*A*) Schematic showing a complex array of stimulus plugs being generated with a laboratory-built robot by aspirating from a 96-well plate filled with various solutions and carrier fluid. (*B*) Schematic drawing showing the sequence of stimulus plugs in the array used for Fig. 2*C* (See section *Fig. 2C*, above, for details). (*C*) Schematic drawing showing the position of the confocal line scan in the wetting layer above substrate for Fig. 2C. (*D*) A time series of line scans showing fluorescence intensity of fluorescein and sulforhodamine 101 delivered to the surface by the chemistrode. Line scans of bright-field and fluorescence are overlaid. Data plotted in Fig. 2*C* are the intensities averaged between the 2 black dashed lines.

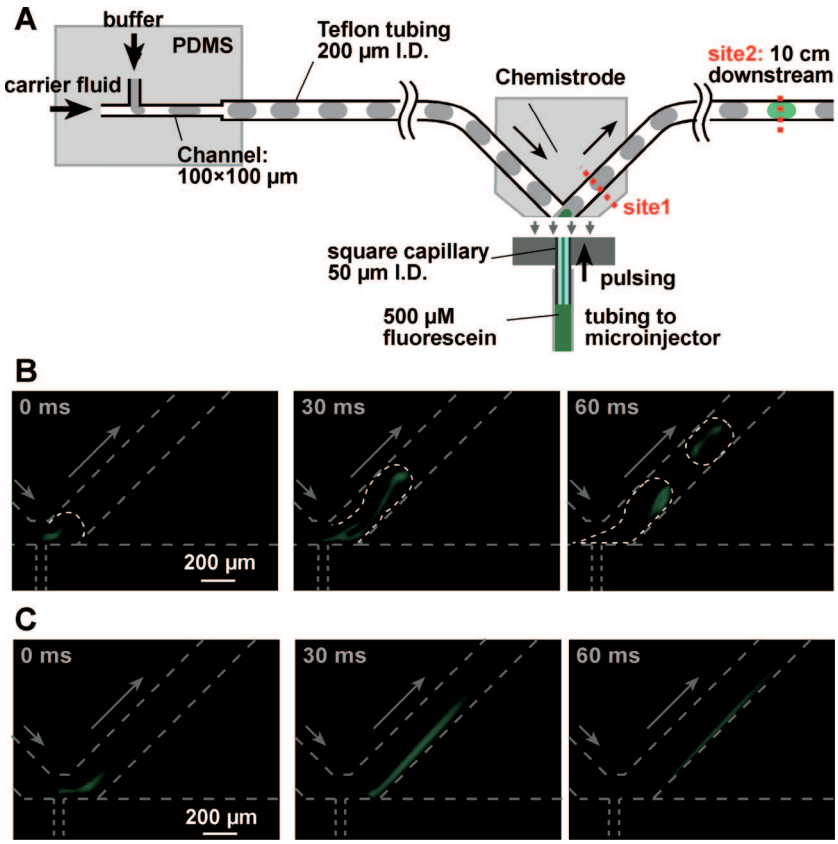

Fig. S4. Experimental setup and data acquisition for Fig. 2*D*. (*A*) Schematic drawing of the setup for generating stimulus plugs, pulsing fluorescein to the PDMS surface by using a microinjector, collecting the fluorescein in response plugs, and measuring fluorescence in the response plugs at sites 1 and 2. (*B*) Microscopic images of chemistrode recording 40-ms pulses of fluorescein. (*C*) Microscopic images of single-phase flow recording 40-ms pulses of fluorescein. Arrows indicate the direction of flow.

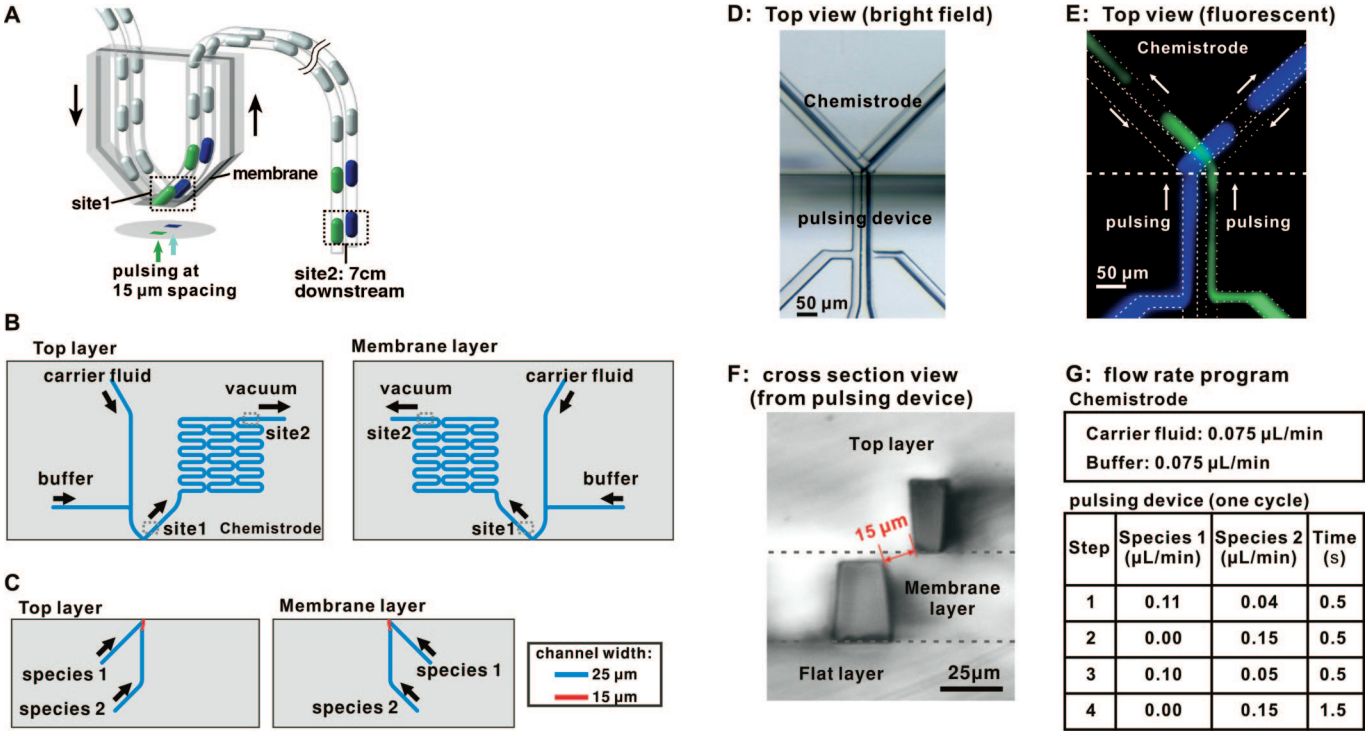

Step	Species 1 (μL/min)	Species 2 (μL/min)	Time (s)
1	0.11	0.04	0.5
2	0.00	0.15	0.5
3	0.10	0.05	0.5
4	0.00	0.15	1.5

Fig. S5. Device design and experimental procedures for Fig. 3. (*A*) Schematic of the experimental design for multilayer chemistrode with 15-μm spatial resolution (see *Device and Methods for Fig. 3* for details). Gray shade represents PDMS membrane between 2 layers. (*B*) Designs for the 2 layers of the chemistrode. The channel features were designed to be 25 μm wide and 25 μm thick. (*C*) Designs for the 2 layers of the pulsing device. Channel features are 25 μm wide and 25 μm (blue line) or 15 μm (red line) thick. The top layer and the membrane layer were aligned to make the tips of pulsing devices $\approx$15 μm apart. (*D*) A bright-field image of the chemistrode brought into contact with the pulsing device. (*E*) Fluorescence image of the chemistrode while recording. Two separate microscopic images obtained with DAPI filter (for MPTS, top layer) and GFP filter (for fluorescein, membrane layer) were overlapped. Fluorescent dyes were pulsed to the surface and recorded by chemistrode with high spatial resolution without cross-contamination. Arrows indicate the direction of flow. (*F*) A image of the cross-section of the pulsing channels. The distance between the closest corners of the 2 pulsing channels are 15 μm. (*G*) Flow rates set with the LabVIEW program for the chemistrode and pulsing device. The flow rates for carrier fluid and aqueous buffer (1$\times$ PBS buffer, pH 7.4) were both 0.075 μL/min. Species 1 (0.4 mM fluorescein or MPTS) and species 2 (1$\times$ PBS buffer, pH 7.4) were pulsed with the cycling program as listed.

A

Solution	1	2	3	4	5
Fraction of sample solution	0	0.08	0.16	0.24	0.32
Fraction of 25 mM HEPES buffer with 0.1% Tween 20	0.2	0.12	0.04	0	0
Fraction of 25 mM HEPES buffer	0.8	0.8	0.8	0.76	0.68
Concentration of Ca2+ (μM)	0	20	40	60	80

B

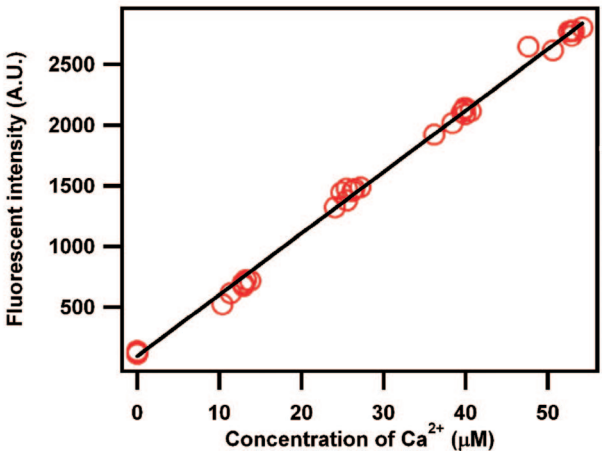

Fig. S6. Method for generating a calibration curve for detecting Ca^{2+}. (*A*) Solutions made to obtain a calibration curve for detecting Ca^{2+}. (*B*) Calibration curve for detecting Ca^{2+}.

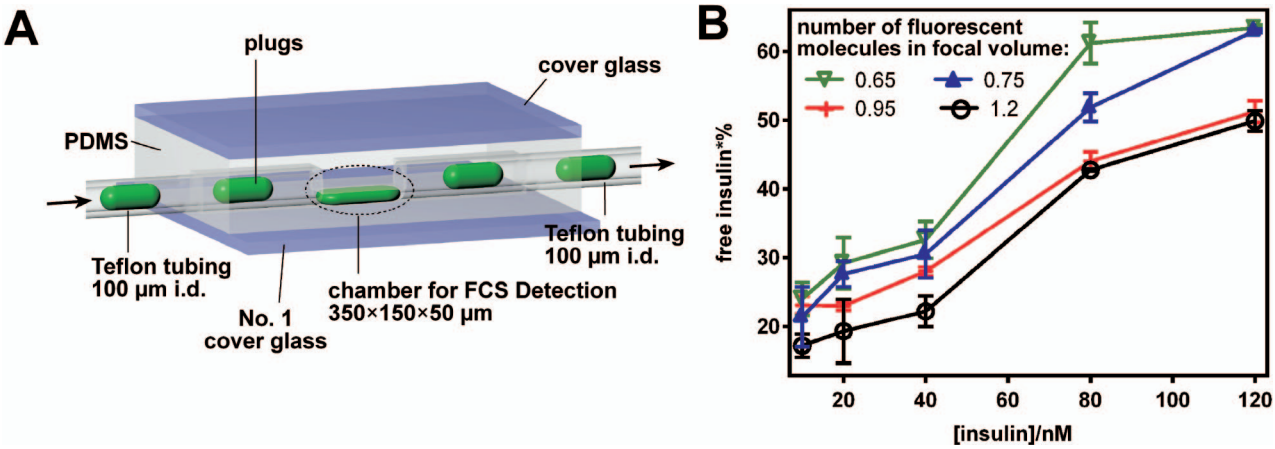

Fig. S7. Device and methods for detecting insulin in response plugs. (*A*) Device for FCS measurements in an array of nanoliter plugs. (*B*) Calibration curves for detecting insulin by FCS. The horizontal axis is the concentration of insulin in the response plug before analyzing reagent was injected. Insulin concentrations below 20 nM or above 120 nM could not be accurately measured due to the limited dynamic range of the immunoassay. The error bars are the difference between 2 parallel measurements.

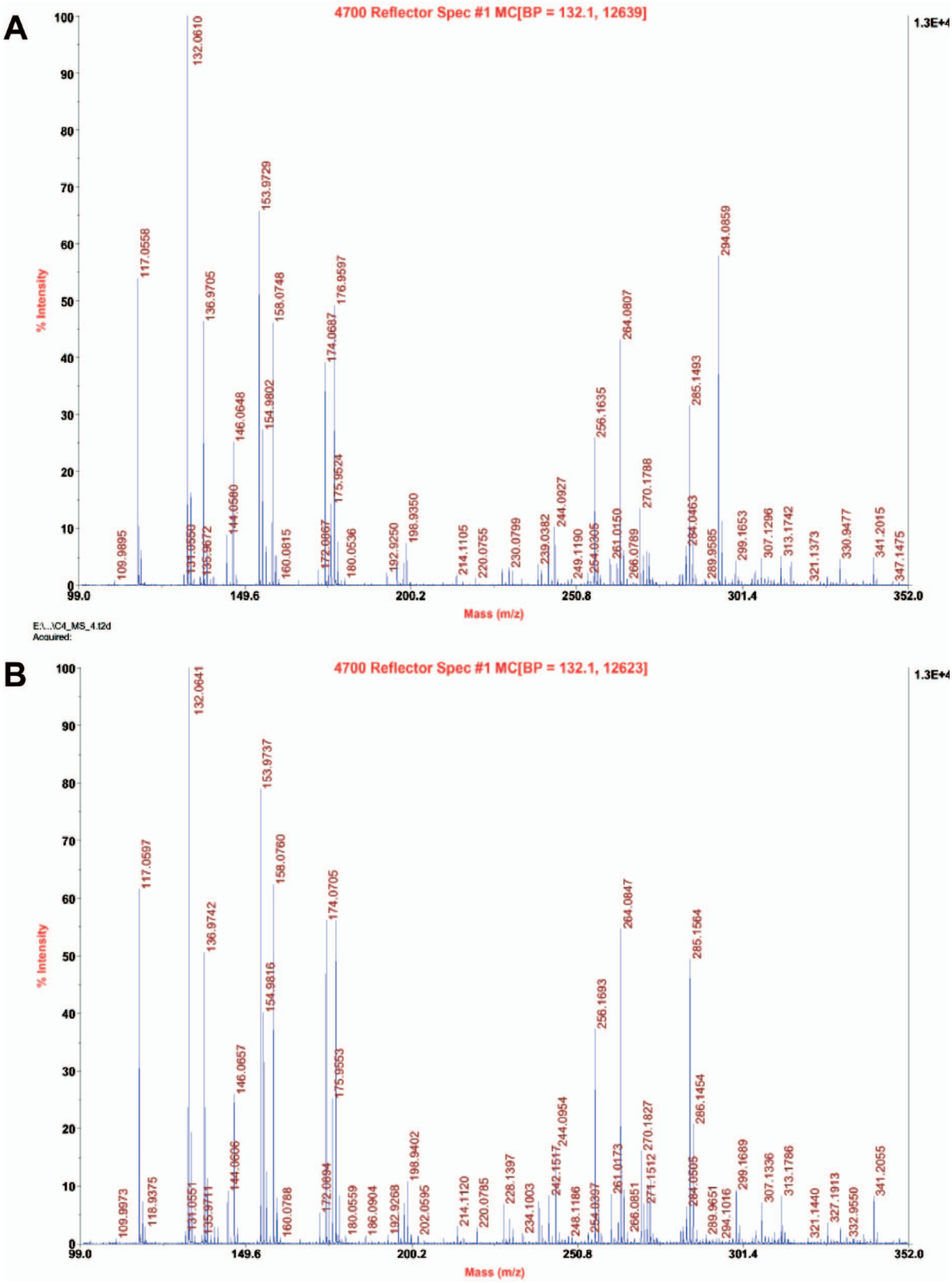

Fig. S8. Representative MALDI-MS spectra. (*A*) A representative MALDI spectrum for a response plug that captured a pulse of sample solution containing glucose. (*B*) A representative MALDI spectrum for a response plug that captured a pulse of buffer containing no glucose.

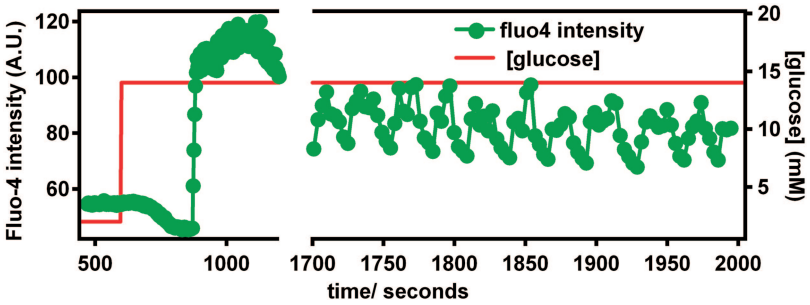

Fig. S9. Characteristic profile and oscillation of intracellular $[Ca^{2+}]_i$ (green) were observed upon stimulation with the chemistrode (red line), indicating normal response of islets.

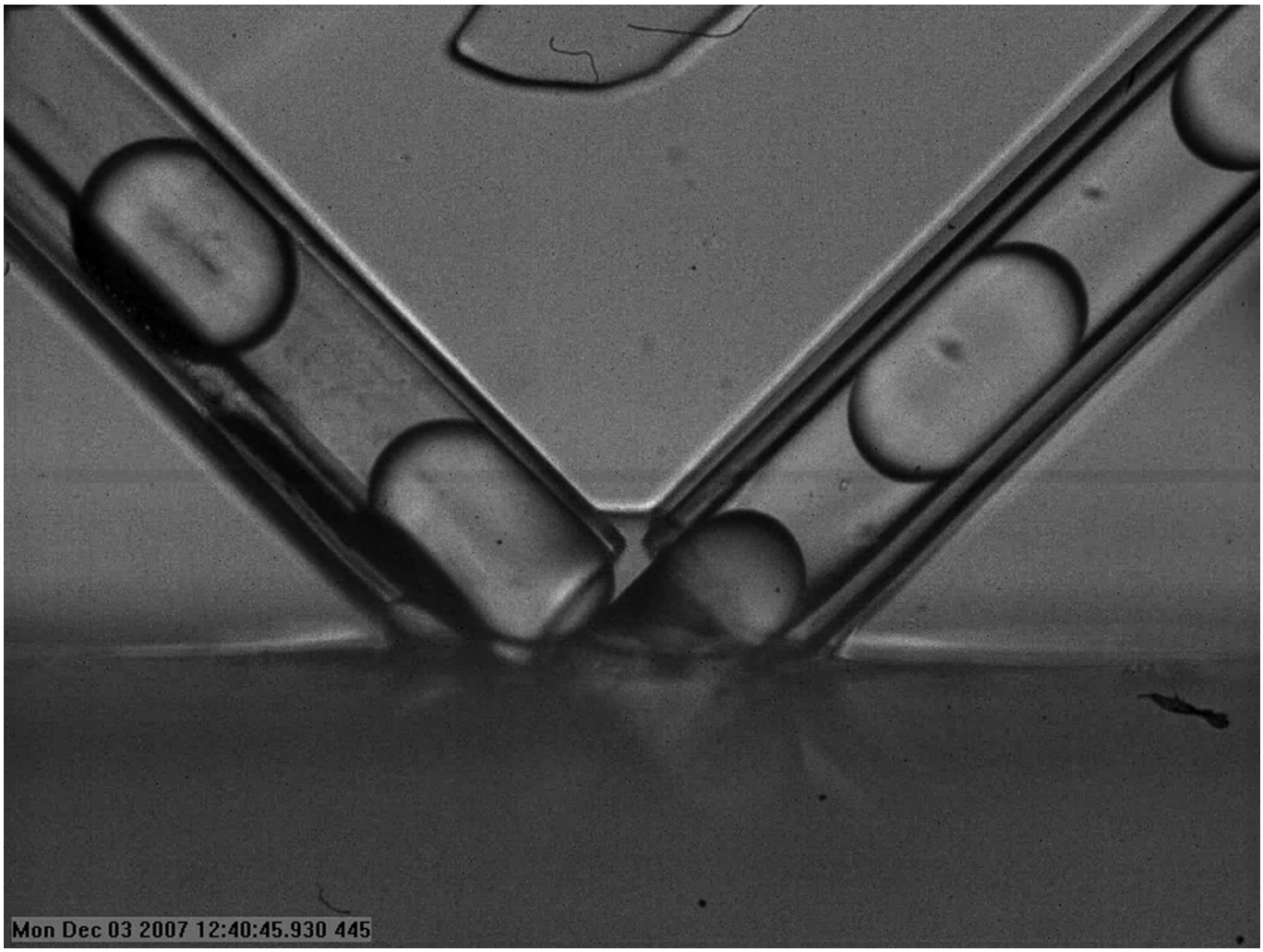

Movie S1. Bright-field images taken at 1,000 frames per second show plugs coalescing with the wetting layer on the substrate and reforming in a chemistrode. The 5.7-s movie corresponds to 0.9 s of real-time imaging data.

Movie S1 (MOV)

Movie S2. Fluorescence images show the mixing and exchange between the wetting layer on the surface and the plugs. Fluorescence images were taken at 500 frames per second. The 19.0-s movie corresponds to 1.2 s of real-time imaging data.

Movie S2 (MOV)

Movie S3. Recording 40-ms fluorescein pulses in substrate with plugs in chemistrode. Fluorescence images were taken at 200 frames per second. The 9.1-s movie corresponds to 1.4 s of real-time imaging data.

Movie S3 (MOV)

Movie S4. Recording of 40-ms fluorescein pulses with single-phase laminar flow. Images were taken at 400 frames per second. The 10.0-s movie corresponds to 1.5 s real-time imaging data.

Movie S4 (MOV)